

Imaging moving targets from scattered waves

This article has been downloaded from IOPscience. Please scroll down to see the full text article.

2008 Inverse Problems 24 035005

(<http://iopscience.iop.org/0266-5611/24/3/035005>)

View [the table of contents for this issue](#), or go to the [journal homepage](#) for more

Download details:

IP Address: 38.107.179.213

The article was downloaded on 21/02/2012 at 23:25

Please note that [terms and conditions apply](#).

Imaging moving targets from scattered waves

Margaret Cheney¹ and Brett Borden²

¹ Department of Mathematical Sciences, Rensselaer Polytechnic Institute, Troy, NY 12180 USA

² Physics Department, Naval Postgraduate School, Monterey, CA 93943 USA

Received 15 August 2007, in final form 25 January 2008

Published 8 April 2008

Online at stacks.iop.org/IP/24/035005

Abstract

We develop a linearized imaging theory that combines the spatial, temporal and spectral aspects of scattered waves. We consider the case of fixed sensors and a general distribution of objects, each undergoing linear motion; thus the theory deals with imaging distributions in phase space. We derive a model for the data that is appropriate for any waveform, and show how it specializes to familiar results in the cases when: (a) the targets are moving slowly, (b) the targets are far from the antennas and (c) narrowband waveforms are used. From these models, we develop a phase-space imaging formula that can be interpreted in terms of filtered backprojection or matched filtering. For this imaging approach, we derive the corresponding point-spread function. We show that special cases of the theory reduce to: (a) range-Doppler imaging, (b) inverse synthetic aperture radar (ISAR), (c) synthetic aperture radar (SAR), (d) Doppler SAR, (e) diffraction tomography and (f) tomography of moving targets. We also show that the theory gives a new SAR imaging algorithm for waveforms with arbitrary ridge-like ambiguity functions.

1. Introduction

Many imaging techniques are based on measurements of scattered waves and, typically, overall image resolution is proportional to the ratio of system aperture to signal wavelength. When the physical (real) aperture is small in comparison with wavelength, an extended ‘effective aperture’ can sometimes be formed analytically: examples include ultrasound, radar, sonar and seismic prospecting. For the most part, these *synthetic-aperture* methods rely on time-delay measurements of impulsive echo wavefronts and assume that the region to be imaged is stationary.

For an imaging region containing moving objects, on the other hand, it is well known that measurements of the Doppler shift can be used to obtain information about velocities. This principle is the foundation of Doppler ultrasound, police radar systems and some moving target indicator (MTI) radar systems. The classical ‘radar ambiguity’ theory [5, 11, 22] for monostatic (backscattering) radar shows that the accuracy to which one can measure the Doppler shift and time delay depends on the transmitted waveform. There is similar theory for the case when a single transmitter and receiver are at different locations [19–21]. Ambiguity

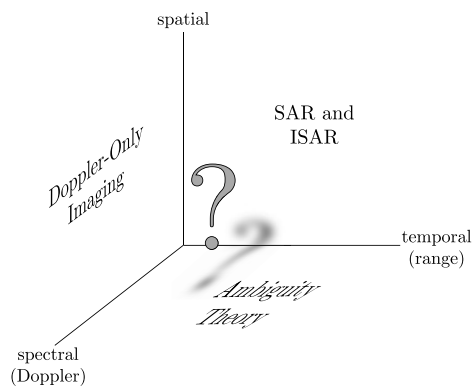


Figure 1. A diagram of various theories that combine spatial, spectral and temporal aspects of scattered waves.

theory appears as the bottom plane in figure 1. Some recent work [3] develops a way to combine range and Doppler information measured at multiple receivers in order to maximize the probability of detection.

In recent years, a number of attempts to develop imaging techniques that can handle moving objects have been proposed. Space-time adaptive processing (STAP) [10] uses a moving multiple-element array together with a real-aperture imaging technique to produce ground moving target indicator (GMTI) image information. Velocity synthetic aperture radar (VSAR) [8] also uses a moving multiple-element array to form a SAR image from each element; then from a comparison of image phases, the system deduces target motion. The paper [15] uses a separate transmitter and receiver together with sequential pulses to estimate target motion from multiple looks. Another technique [16] uses backscattering data from a single sensor to identify rigid-body target motion, which is then used to form a three-dimensional image. Other work [12] extracts target velocity information by exploiting the smearing that appears in SAR images when the along-track target velocity is incorrectly identified. All of these techniques make use of the so-called start-stop approximation, in which a target in motion is assumed to be momentarily stationary while it is being interrogated by a radar pulse. In other words, Doppler measurements are not actually made by these systems. Thus these methods appear on the back plane of figure 1.

Imaging techniques that rely on Doppler data are generally real-aperture systems, and provide spatial information with very low resolution. A synthetic-aperture approach to imaging from a moving sensor and a fixed target was developed in [2]. This Doppler imaging method appears on the left plane of figure 1. An approach that explicitly considers the Doppler shift is Tomography of Moving Targets (TMT) [9], which uses multiple transmitters and receivers (together with matched-filter processing) to both form an image and find the velocity.

Below we develop a theory that shows how to unify these different approaches. In the process, we will demonstrate how we can fuse the spatial, temporal and spectral aspects of scattered-field-based imaging. The present discussion deals with the case of fixed distributed sensors, although our results include monostatic configurations (in which a single transmitter and receiver are co-located) as a special case. Methods for imaging stationary scenes in the case when the transmitter and receiver are not co-located have been particularly well developed in the geophysics literature [1] and have also been explored in the radar literature [19–21].

In section 2, we develop a physics-based mathematical model that incorporates not only the waveform and wave propagation effects due to moving scatterers, but also the

effects of spatial diversity of transmitters and receivers. In section 3, we show how a matched-filtering technique produces images that depend on target velocity, and we relate the resulting point-spread function to the classical wideband and narrowband radar ambiguity functions. We also work out the special cases of far-field imaging and narrowband imaging of slowly-moving targets. Finally, in section 4, we show that for special cases, the theory developed in section 3 reduces to familiar results. We also show that the theory provides a new imaging algorithm for certain waveforms.

2. Model for data

We model wave propagation and scattering by the scalar wave equation for the wavefield $\psi(t, \mathbf{x})$ due to a source waveform $\check{s}(t, \mathbf{x})$,

$$[\nabla^2 - c^{-2}(t, \mathbf{x})\partial_t^2]\psi(t, \mathbf{x}) = \check{s}(t, \mathbf{x}). \quad (1)$$

For example, a single isotropic source located at \mathbf{y} transmitting the waveform $s(t)$ starting at time $t = -T_y$ could be modeled as $\check{s}(t, \mathbf{x}) = \delta(\mathbf{x} - \mathbf{y})s_y(t + T_y)$, where the subscript \mathbf{y} reminds us that different transmitters could transmit different waveforms. For simplicity, in this paper we consider only localized isotropic sources; the work can easily be extended to more realistic antenna models [13].

A single scatterer moving at velocity \mathbf{v} corresponds to an index-of-refraction distribution $n^2(\mathbf{x} - \mathbf{v}t)$:

$$c^{-2}(t, \mathbf{x}) = c_0^{-2}[1 + n^2(\mathbf{x} - \mathbf{v}t)], \quad (2)$$

where c_0 denotes the speed in the stationary background medium (here assumed constant). For radar, c_0 is the speed of light in vacuum. We write $q_v(\mathbf{x} - \mathbf{v}t) = c_0^{-2}n^2(\mathbf{x} - \mathbf{v}t)$. To model multiple moving scatterers, we let $q_v(\mathbf{x} - \mathbf{v}t) d^3x d^3v$ be the corresponding quantity for the scatterers in the volume $d^3x d^3v$ centered at (\mathbf{x}, \mathbf{v}) . Thus q_v is the distribution, at time $t = 0$, of scatterers moving with velocity \mathbf{v} . Consequently, the scatterers in the spatial volume d^3x (at \mathbf{x}) give rise to

$$c^{-2}(t, \mathbf{x}) = c_0^{-2} + \int q_v(\mathbf{x} - \mathbf{v}t) d^3v. \quad (3)$$

We note that the physical interpretation of q_v involves a choice of a time origin. A choice that is particularly appropriate, in view of our assumption about linear target velocities, is a time during which the wave is interacting with targets of interest. This implies that the activation of the antenna at \mathbf{y} takes place at a negative time which we denote by $-T_y$; we write $\check{s}(t, \mathbf{x}) = s_y(t + T_y)\delta(\mathbf{x} - \mathbf{y})$. The wave equation corresponding to (3) is then

$$\left[\nabla^2 - c_0^{-2}\partial_t^2 - \int q_v(\mathbf{x} - \mathbf{v}t) d^3v \partial_t^2 \right] \psi(t, \mathbf{x}) = s_y(t + T_y)\delta(\mathbf{x} - \mathbf{y}). \quad (4)$$

2.1. The transmitted field

We consider the transmitted field ψ^{in} in the absence of any scatterers; ψ^{in} satisfies the version of equation (1) in which c is simply the constant background speed c_0 , namely

$$[\nabla^2 - c_0^{-2}\partial_t^2]\psi^{\text{in}}(t, \mathbf{x}, \mathbf{y}) = s_y(t + T_y)\delta(\mathbf{x} - \mathbf{y}). \quad (5)$$

Henceforth we drop the subscript on c . We use the Green's function g , which satisfies

$$[\nabla^2 - c_0^{-2}\partial_t^2]g(t, \mathbf{x}) = -\delta(t)\delta(\mathbf{x})$$

and is given by

$$g(t, |\mathbf{x}|) = \frac{\delta(t - |\mathbf{x}|/c)}{4\pi |\mathbf{x}|} = \frac{1}{8\pi^2 |\mathbf{x}|} \int e^{-i\omega(t - |\mathbf{x}|/c)} d\omega, \quad (6)$$

where we have used $2\pi\delta(t) = \int \exp(-i\omega t) d\omega$. We use (6) to solve (5), obtaining

$$\begin{aligned} \psi^{\text{in}}(t, \mathbf{x}, \mathbf{y}) &= - \int g(t - t', |\mathbf{x} - \mathbf{y}|) s_{\mathbf{y}}(t' + T_{\mathbf{y}}) \delta(\mathbf{x} - \mathbf{y}) dt' d\mathbf{y} \\ &= - \frac{s_{\mathbf{y}}(t + T_{\mathbf{y}} - |\mathbf{x} - \mathbf{y}|/c)}{4\pi |\mathbf{x} - \mathbf{y}|}. \end{aligned} \quad (7)$$

2.2. The scattered field

We write $\psi = \psi^{\text{in}} + \tilde{\psi}^{\text{sc}}$, which converts (1) into

$$[\nabla^2 - c_0^{-2} \partial_t^2] \tilde{\psi}^{\text{sc}} = \int q_v(\mathbf{x} - \mathbf{v}t) d^3 v \partial_t^2 \psi. \quad (8)$$

The map $q \mapsto \tilde{\psi}^{\text{sc}}$ can be linearized by replacing the full field ψ on the right-hand side of (8) by ψ^{in} . This substitution results in the Born approximation ψ^{sc} for the scattered field $\tilde{\psi}^{\text{sc}}$ at the location \mathbf{z} ,

$$\begin{aligned} \psi^{\text{sc}}(t, \mathbf{z}) &= - \int g(t - t', |\mathbf{z} - \mathbf{x}|) \int q_v(\mathbf{x} - \mathbf{v}t') d^3 v \partial_t^2 \psi^{\text{in}}(t', \mathbf{x}) dt' d^3 x \\ &= \int \frac{\delta(t - t' - |\mathbf{z} - \mathbf{x}|/c)}{4\pi |\mathbf{z} - \mathbf{x}|} \int q_v(\mathbf{x} - \mathbf{v}t') d^3 v \partial_t^2 \frac{s_{\mathbf{y}}(t' + T_{\mathbf{y}} - |\mathbf{x} - \mathbf{y}|/c)}{4\pi |\mathbf{x} - \mathbf{y}|} d^3 x dt'. \end{aligned} \quad (9)$$

In equation (9), we make the change of variables $\mathbf{x} \mapsto \mathbf{x}' = \mathbf{x} - \mathbf{v}t'$ (i.e., change to the frame of reference in which the scatterer q_v is fixed) to obtain

$$\begin{aligned} \psi^{\text{sc}}(t, \mathbf{z}) &= \int \frac{\delta(t - t' - |\mathbf{x}' + \mathbf{v}t' - \mathbf{z}|/c)}{4\pi |\mathbf{x}' + \mathbf{v}t' - \mathbf{z}|} \\ &\quad \times \int q_v(\mathbf{x}') \frac{\ddot{s}_{\mathbf{y}}(t' + T_{\mathbf{y}} - |\mathbf{x}' + \mathbf{v}t' - \mathbf{y}|/c)}{4\pi |\mathbf{x}' + \mathbf{v}t' - \mathbf{y}|} d^3 x' d^3 v dt'. \end{aligned} \quad (10)$$

The physical interpretation of (10) is as follows: the wave that emanates from \mathbf{y} at time $-T_{\mathbf{y}}$ encounters a target at time t' . This target, during the time interval $[0, t']$, has moved from \mathbf{x} to $\mathbf{x} + \mathbf{v}t'$. The wave scatters with strength $q_v(\mathbf{x})$, and then propagates from position $\mathbf{x} + \mathbf{v}t'$ to \mathbf{z} , arriving at time t .

Henceforth we will drop the primes on \mathbf{x} . We introduce the notation

$$\mathbf{R}_{\mathbf{x}, \mathbf{z}}(t) = \mathbf{x} + \mathbf{v}t - \mathbf{z} \quad R = |\mathbf{R}|, \quad \text{and} \quad \widehat{\mathbf{R}} = \mathbf{R}/R. \quad (11)$$

To evaluate the t' integral of (10), we denote by $t' = \bar{t}_{\mathbf{x}, \mathbf{v}}(t)$ the implicit solution of $t - t' - R_{\mathbf{x}, \mathbf{z}}(t')/c = 0$, i.e.,

$$0 = t - \bar{t}_{\mathbf{x}, \mathbf{v}}(t) - R_{\mathbf{x}, \mathbf{z}}(\bar{t}_{\mathbf{x}, \mathbf{v}}(t))/c. \quad (12)$$

The time $\bar{t}_{\mathbf{x}, \mathbf{v}}(t)$ is the time when the wave reaching the receiver at \mathbf{z} at time t interacted with the target that, at time $t = 0$, was located at \mathbf{x} . This target, at time $\bar{t}_{\mathbf{x}, \mathbf{v}}(t)$, is actually located at $\mathbf{x} + \mathbf{v}\bar{t}_{\mathbf{x}, \mathbf{v}}(t)$. With this notation, equation (10) becomes

$$\begin{aligned} \psi^{\text{sc}}(t, \mathbf{z}) &= \int \frac{\ddot{s}_{\mathbf{y}}[\bar{t}_{\mathbf{x}, \mathbf{v}}(t) + T_{\mathbf{y}} - R_{\mathbf{x}, \mathbf{y}}(\bar{t}_{\mathbf{x}, \mathbf{v}}(t))/c]}{(4\pi)^2 R_{\mathbf{x}, \mathbf{z}}(\bar{t}_{\mathbf{x}, \mathbf{v}}(t)) R_{\mathbf{x}, \mathbf{y}}(\bar{t}_{\mathbf{x}, \mathbf{v}}(t))} q_v(\mathbf{x}) d^3 x d^3 v \\ &= \int \frac{\ddot{s}_{\mathbf{y}}(t + T_{\mathbf{y}} - R_{\mathbf{x}, \mathbf{z}}(\bar{t}_{\mathbf{x}, \mathbf{v}}(t))/c - R_{\mathbf{x}, \mathbf{y}}(\bar{t}_{\mathbf{x}, \mathbf{v}}(t))/c)}{(4\pi)^2 R_{\mathbf{x}, \mathbf{z}}(\bar{t}_{\mathbf{x}, \mathbf{v}}(t)) R_{\mathbf{x}, \mathbf{y}}(\bar{t}_{\mathbf{x}, \mathbf{v}}(t))} q_v(\mathbf{x}) d^3 x d^3 v, \end{aligned} \quad (13)$$

where, in the second line, we have used (12) to write the argument of \ddot{s} in a more symmetrical form.

Expression (13) is appropriate under very general circumstances. In particular, this formula applies to wide-beam imaging where the commonly-used far-field approximations do not apply. Equation (13) also applies to rapidly moving targets, where the start-stop approximation is not valid, and to very distant targets. Finally, this result can be used for arbitrary transmitted waveforms.

2.2.1. The slow-mover case. Here we assume that $|v|t$ and $k|v|^2t^2$ are much less than $|x - z|$ and $|x - y|$, where $k = \omega_{\max}/c$, with ω_{\max} being the (effective) maximum angular frequency of the signal s_y . In this case, we have

$$R_{x,z}(t) = |z - (x + vt)| = R_{x,z}(0) + \widehat{R}_{x,z}(0) \cdot vt + O\left(\frac{|vt|^2}{R_{x,z}}\right), \quad (14)$$

where $\mathbf{R}_{x,z}(0) = \mathbf{x} - \mathbf{z}$, $R_{x,z}(0) = |\mathbf{R}_{x,z}(0)|$, and $\widehat{R}_{x,z}(0) = \mathbf{R}_{x,z}(0)/R_{x,z}(0)$. With (14), equation (12) becomes

$$\bar{t}_{x,v} \approx t - \left[\frac{R_{x,z}(0)}{c} + \widehat{R}_{x,z}(0) \cdot \frac{v\bar{t}_{x,v}}{c} \right], \quad (15)$$

which can be solved explicitly to obtain

$$\bar{t}_{x,v}(t) \approx \frac{t - R_{x,z}(0)/c}{1 + \widehat{R}_{x,z}(0) \cdot v/c}. \quad (16)$$

The argument of \bar{s} in equation (13) is then

$$\begin{aligned} \bar{t}_{x,v}(t) + T_y - \frac{R_{x,y}(\bar{t}_{x,v}(t))}{c} &\approx \bar{t}_{x,v}(t) + T_y - \left(\frac{R_{x,y}(0)}{c} + \frac{\widehat{R}_{x,y}(0) \cdot v}{c} \bar{t}_{x,v}(t) \right) \\ &= \frac{1 - \widehat{R}_{x,y}(0) \cdot v/c}{1 + \widehat{R}_{x,z}(0) \cdot v/c} \left(t - \frac{R_{x,z}(0)}{c} \right) - \frac{R_{x,y}(0)}{c} + T_y. \end{aligned} \quad (17)$$

The time dilation

$$\tilde{\alpha}_{x,v} = \frac{1 - \widehat{R}_{x,y}(0) \cdot v/c}{1 + \widehat{R}_{x,z}(0) \cdot v/c} \quad (18)$$

is the *Doppler scale factor*, which, as we see below, is closely related to the Doppler shift.

With (17) and the notation (18), equation (13) becomes

$$\psi_s^{\text{sc}}(t, z, \mathbf{y}) = \int \frac{\tilde{s}_y[\tilde{\alpha}_{x,v}(t - R_{x,z}(0)/c) - R_{x,y}(0)/c + T_y]}{(4\pi)^2 R_{x,z}(0) R_{x,y}(0)} q_v(\mathbf{x}) d^3x d^3v. \quad (19)$$

2.2.2. The slow-mover, narrow-band case. Many radar systems use a *narrowband waveform*, defined by

$$s_y(t) = \tilde{s}_y(t) e^{-i\omega_y t}, \quad (20)$$

where $\tilde{s}(t, \mathbf{y})$ is *slowly varying*, as a function of t , in comparison with $\exp(-i\omega_y t)$, where ω_y is the carrier frequency for the transmitter at position \mathbf{y} .

For the waveform (20), equation (19) becomes

$$\begin{aligned} \psi_N^{\text{sc}}(t, z, \mathbf{y}) &= - \int \frac{\omega_y^2}{(4\pi)^2 R_{x,z}(0) R_{x,y}(0)} e^{-i\omega_y[\tilde{\alpha}_{x,v}(t - R_{x,z}(0)/c) - R_{x,y}(0)/c + T_y]} \\ &\quad \times \tilde{s}_y(\tilde{\alpha}_{x,v}(t - R_{x,z}(0)/c) - R_{x,y}(0)/c + T_y) q_v(\mathbf{x}) d^3x d^3v \\ &\approx - \int \frac{\omega_y^2 e^{i\varphi_{x,v}} e^{-i\omega_y \tilde{\alpha}_{x,v} t}}{(4\pi)^2 R_{x,z}(0) R_{x,y}(0)} \tilde{s}_y(t + T_y - (R_{x,z}(0) + R_{x,y}(0))/c) q_v(\mathbf{x}) d^3x d^3v. \end{aligned} \quad (21)$$

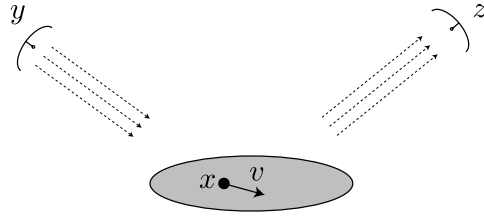


Figure 2. The geometry in the far-field case. This shows a case in which the scene is not too large.

Here we have used the fact that s is slowly varying to replace $\alpha_{x,v}$ by 1 in the argument of s , and we have collected the time-independent terms in the exponent into the quantity

$$\varphi_{x,v} = k_y [R_{x,y}(0) - T_y + \tilde{\alpha}_{x,v} R_{x,z}(0)], \tag{22}$$

where $k_y = \omega_y/c$.

If we write the Doppler scale factor (18) as $\tilde{\alpha}_{x,v} \approx 1 + \beta_{x,v}$, where

$$\beta_{x,v} = -(\hat{\mathbf{R}}_{x,y}(0) + \hat{\mathbf{R}}_{x,z}(0)) \cdot \mathbf{v}/c, \tag{23}$$

then the quantity $\omega_y \beta_{x,v}$ is the *Doppler shift*. We note that the Doppler shift depends on the bistatic bisector vector $\hat{\mathbf{R}}_{x,y}(0) + \hat{\mathbf{R}}_{x,z}(0)$.

With equation (23), we recognize (21) as the familiar superposition of time-delayed and Doppler-shifted copies of the transmitted waveform.

2.2.3. *The far-field case.* A common situation is the one in which the transmitter-to-target and target-to-receiver distances are large in comparison with the scene dimensions (see figure 2). We take the origin of coordinates to be at the scene center. Then, in the so-called far-field approximation, $|\mathbf{x} + \mathbf{v}t'|$ and $k|\mathbf{x} + \mathbf{v}t'|^2$ are assumed to be much less than either $|z|$ or $|y|$, where k again corresponds to the (effective) maximum wave number for the signal s_y , and we have

$$R_{x,z}(t) = |z - (\mathbf{x} + \mathbf{v}t)| = |z| - \hat{\mathbf{z}} \cdot (\mathbf{x} + \mathbf{v}t) + O\left(\frac{|\mathbf{x} + \mathbf{v}t|^2}{|z|}\right). \tag{24}$$

In this approximation, equation (12) reduces to

$$\bar{t}_{x,v} \approx t - \left[\frac{|z|}{c} - \hat{\mathbf{z}} \cdot \frac{\mathbf{x} + \mathbf{v}\bar{t}_{x,v}}{c} \right], \tag{25}$$

which can be solved explicitly to yield

$$\bar{t}_{x,v}(t) \approx \frac{t - |z|/c + \hat{\mathbf{z}} \cdot \mathbf{x}/c}{1 - \hat{\mathbf{z}} \cdot \mathbf{v}/c}. \tag{26}$$

The argument of \bar{s} in equation (13) is then

$$\begin{aligned} t + T_y - \frac{R_{x,z}(\bar{t}_{x,v}(t))}{c} - \frac{R_{x,y}(\bar{t}_{x,v}(t))}{c} &\approx \bar{t}_{x,v}(t) - \left(\frac{|y|}{c} - \frac{\hat{\mathbf{y}} \cdot \mathbf{x}}{c} - \frac{\hat{\mathbf{y}} \cdot \mathbf{v}}{c} \bar{t}_{x,v}(t) \right) + T_y \\ &= \frac{1 + \hat{\mathbf{y}} \cdot \mathbf{v}/c}{1 - \hat{\mathbf{z}} \cdot \mathbf{v}/c} \left(t - \frac{|z|}{c} + \frac{\hat{\mathbf{z}} \cdot \mathbf{x}}{c} \right) - \frac{|y|}{c} + \frac{\hat{\mathbf{y}} \cdot \mathbf{x}}{c} + T_y. \end{aligned} \tag{27}$$

We see that when $|\mathbf{v}|/c \ll 1$, the Doppler scale factor becomes

$$\alpha_v = \frac{1 + \hat{\mathbf{y}} \cdot \mathbf{v}/c}{1 - \hat{\mathbf{z}} \cdot \mathbf{v}/c} \approx 1 + (\hat{\mathbf{y}} + \hat{\mathbf{z}}) \cdot \mathbf{v}/c. \tag{28}$$

We note that the signs here appear different from those in equation (18) because $\mathbf{R}_{\mathbf{x},\mathbf{z}}(0) = \mathbf{x} - \mathbf{z}$ points in a direction approximately opposite to $\mathbf{z} = \mathbf{z} - \mathbf{0}$. The scattered field is

$$\psi_{\text{f}}^{\text{sc}}(t, \mathbf{z}, \mathbf{y}) = \int \frac{\tilde{s}_{\mathbf{y}}[\alpha_v(t - |\mathbf{z}|/c + \hat{\mathbf{z}} \cdot \mathbf{x}/c) - |\mathbf{y}|/c + \hat{\mathbf{y}} \cdot \mathbf{x}/c + T_{\mathbf{y}}]}{(4\pi)^2 |\mathbf{z}| |\mathbf{y}|} q_v(\mathbf{x}') d^3 x d^3 v. \quad (29)$$

2.2.4. The far-field, narrowband case. With a narrowband waveform (20) and the far-field approximation (24), equation (29) becomes

$$\begin{aligned} \psi_{\text{fN}}^{\text{sc}}(t, \mathbf{z}, \mathbf{y}) &= -\frac{\omega_y^2}{(4\pi)^2 |\mathbf{z}| |\mathbf{y}|} \int \tilde{s}_{\mathbf{y}}(t - |\mathbf{z}|/c + \hat{\mathbf{z}} \cdot \mathbf{x}/c - |\mathbf{y}|/c + \hat{\mathbf{y}} \cdot \mathbf{x}/c + T_{\mathbf{y}}) \\ &\quad \times \exp(-i\omega_y[\alpha_v(t - |\mathbf{z}|/c + \hat{\mathbf{z}} \cdot \mathbf{x}/c) - |\mathbf{y}|/c + \hat{\mathbf{y}} \cdot \mathbf{x}/c + T_{\mathbf{y}}]) q_v(\mathbf{x}) d^3 x d^3 v \\ &\approx -\frac{\omega_y^2}{(4\pi)^2 |\mathbf{z}| |\mathbf{y}|} \int \exp(i\varphi_{\mathbf{x},v}^{\text{f}}) \exp(-i\omega_y \alpha_v t) \\ &\quad \times \tilde{s}_{\mathbf{y}}(t + T_{\mathbf{y}} - (|\mathbf{z}| - \hat{\mathbf{z}} \cdot \mathbf{x} + |\mathbf{y}| - \hat{\mathbf{y}} \cdot \mathbf{x})/c) q_v(\mathbf{x}) d^3 x d^3 v, \end{aligned} \quad (30)$$

where $\varphi_{\mathbf{x},v}^{\text{f}} = -\omega_y[\alpha_v(-|\mathbf{z}| + \hat{\mathbf{z}} \cdot \mathbf{x}) - |\mathbf{y}| + \hat{\mathbf{y}} \cdot \mathbf{x}]/c$.

If the transmitter is activated at times $-T_{\mathbf{y}} = -|\mathbf{y}|/c$, so that the transmitted wave arrives at the scene center at the time $t = 0$, and if we evaluate $\psi_{\text{fN}}^{\text{sc}}$ at $t' = t - |\mathbf{z}|/c$, we have

$$\psi_{\text{fN}}^{\text{sc}}(t', \mathbf{z}, \mathbf{y}) = \frac{-\omega_y^2}{(4\pi)^2 |\mathbf{z}| |\mathbf{y}|} \int e^{i\tilde{\varphi}_{\mathbf{x},v}} e^{-i\omega_y \alpha_v t'} \tilde{s}_{\mathbf{y}}(t' + (\hat{\mathbf{z}} + \hat{\mathbf{y}}) \cdot \mathbf{x}/c) q_v(\mathbf{x}) d^3 x d^3 v, \quad (31)$$

where

$$\tilde{\varphi}_{\mathbf{x},v} = -\omega_y[\alpha_v \hat{\mathbf{z}} + \hat{\mathbf{y}}] \cdot \mathbf{x}/c \quad (32)$$

Again if we write $\alpha_v = 1 + \beta_v$, where $\beta_v = (\hat{\mathbf{y}} + \hat{\mathbf{z}}) \cdot \mathbf{v}/c$, we see that equation (31) is a superposition of delayed and Doppler-shifted versions of the transmitted signal.

Much previous work has dealt with the case of far-field, single-frequency imaging of a stationary scene. For a stationary scene ($\mathbf{v} = 0$, which implies $\alpha_v = 1$), and a single frequency $\omega_y = \omega_0$ (which corresponds to $\tilde{s} = 1$), (31) reduces to the well-known expression

$$\psi_{\omega_0}^{\infty}(t, \mathbf{z}, \mathbf{y}) \approx \frac{e^{-ik_0 t}}{(4\pi)^2 |\mathbf{z}| |\mathbf{y}|} F_{\infty}(\hat{\mathbf{y}}, \hat{\mathbf{z}}), \quad (33)$$

where the (Born-approximated) far-field pattern or scattering amplitude is

$$F_{\infty}(\hat{\mathbf{y}}, \hat{\mathbf{z}}) = \int e^{-ik_0(\hat{\mathbf{z}} + \hat{\mathbf{y}}) \cdot \mathbf{x}} q(\mathbf{x}) d^3 x, \quad (34)$$

where $k_0 = \omega_0/c$. We note that our incident-wave direction convention (from target to transmitter) is the opposite of that used in the classical scattering theory literature (which uses transmitter to target).

3. Imaging via a filtered adjoint

We now address the question of extracting information from the scattered waveform described by equation (13).

Our image formation algorithm depends on the data we have available. In general, we form a (coherent) image as a filtered adjoint, but the variables we integrate over depend on whether we have multiple transmitters, multiple receivers and/or multiple frequencies. The number of variables we integrate over, in turn, determines how many image dimensions we can hope to reconstruct. If our data depends on two variables, for example, then we can

hope to reconstruct a two-dimensional scene; in this case the scene is commonly assumed to lie on a known surface. If, in addition, we want to reconstruct two-dimensional velocities, then we are seeking a four-dimensional image and thus we will require data depending on at least four variables. More generally, determining a distribution of positions in space and the corresponding three-dimensional velocities means that we seek to form an image in a six-dimensional phase space.

3.1. Imaging formula in the general case

We form an image $I(\mathbf{p}, \mathbf{u})$ of the objects with velocity \mathbf{u} that, at time $t = 0$, were located at position \mathbf{p} . Thus $I(\mathbf{p}, \mathbf{u})$ is constructed to be an approximation to $q_{\mathbf{u}}(\mathbf{p})$. The strategy for the imaging process is to write the data in terms of a Fourier integral operator $\mathcal{F} : q_{\mathbf{v}} \mapsto \psi^{\text{sc}}$, and then find an approximate inverse for \mathcal{F} .

In the general case, we write the data (13) as

$$\psi^{\text{sc}}(t, \mathbf{z}, \mathbf{y}) = - \int \frac{(i\omega')^2 e^{-i\omega'[\bar{r}_{x,v}(t)+T_y-R_{x,y,v}(\bar{r}_{x,v}(t))/c]}}{2^5\pi^3 R_{x,z,v}(\bar{r}_{x,v}(t))R_{x,y,v}(\bar{r}_{x,v}(t))} S_{\mathbf{y}}(\omega') d\omega' q_{\mathbf{v}}(\mathbf{x}_q) d^3x d^3v, \quad (35)$$

where we have written $s_{\mathbf{y}}(t)$ in terms of its inverse Fourier transform

$$s_{\mathbf{y}}(t) = \frac{1}{2\pi} \int e^{-i\omega't} S_{\mathbf{y}}(\omega') d\omega'. \quad (36)$$

We note that by the Paley–Weiner theorem, S is analytic since it is the inverse Fourier transform of the finite-duration waveform s .

The corresponding imaging operation is a filtered version of the formal adjoint of the ‘forward’ operator \mathcal{F} . Thus we form the phase-space image $I(\mathbf{p}, \mathbf{u})$ as

$$I(\mathbf{p}, \mathbf{u}) = \int e^{i\omega[\bar{r}_{p,u}(t)+T_y-R_{p,y}(\bar{r}_{p,u}(t))/c]} Q(\omega, t, \mathbf{p}, \mathbf{u}, \mathbf{z}, \mathbf{y}) d\omega \psi^{\text{sc}}(t, \mathbf{z}, \mathbf{y}) dt d^n z d^m y, \quad (37)$$

where $n = 1, 2$ or 3 , depending on the receiver configuration, and $m = 1, 2$ or 3 , depending on the transmitter configuration. This image reconstruction operator can be interpreted in terms of filtered backpropagation, where Q is the filter.

The specific choice of filter is dictated by various considerations [1, 23]; here we make choices that connect the resulting formulae with familiar theories. In particular, we take the filter Q to be

$$Q(\omega, t, \mathbf{p}, \mathbf{u}, \mathbf{z}, \mathbf{y}) = \frac{(4\pi)^2}{(i\omega)^2} R_{p,z}(\bar{r}_{p,u}(t)) R_{p,y}(\bar{r}_{p,u}(t)) S_{\mathbf{y}}^*(\omega) J(\omega, \mathbf{p}, \mathbf{u}, \mathbf{z}, \mathbf{y}) \alpha_{p,u}(t), \quad (38)$$

a choice which leads (below) to the matched filter. The matched filter is well known [22] to be the optimal filter for enhancing signal to noise in the presence of white Gaussian noise. The quantity J depends on the geometry and is chosen (see below) to compensate for a certain Jacobian that appears; α is the Doppler scale factor for the point \mathbf{p}, \mathbf{u} and is defined by

$$\alpha_{p,u}(t) = \frac{1 - \widehat{\mathbf{R}}_{p,y}(\bar{r}_{p,u}(t)) \cdot \mathbf{u}/c}{1 + \widehat{\mathbf{R}}_{p,z}(\bar{r}_{p,u}(t)) \cdot \mathbf{u}/c}. \quad (39)$$

In allowing (37) and (38) to depend on the transmitter \mathbf{y} , we are implicitly assuming that we can identify the part of the signal that is due to the transmitter at \mathbf{y} . In the case of multiple transmitters, this identification can be accomplished, for example, by having

different transmitters operate at different frequencies or, possibly, by quasi-orthogonal pulse-coding schemes. We are also assuming a coherent system, i.e., that a common time clock is available to all sensors.

For a limited number of discrete receivers (or transmitters), the integral over z (or y) in (37) reduces to a sum.

Interpretation of imaging as matched filtering. In the case when the geometrical factor $\tilde{J} = J/\omega^2$ is independent of ω , we can use (36) to write the imaging operation of equation (37) as

$$\begin{aligned} I(\mathbf{p}, \mathbf{u}) &= -(4\pi)^2 \int s_y^* [\bar{t}_{p,u}(t) + T_y - R_{p,y}(\bar{t}_{p,u}(t))/c] R_{p,z}(\bar{t}_{p,u}(t)) R_{p,y}(\bar{t}_{p,u}(t)) \\ &\quad \times \tilde{J}(\mathbf{p}, \mathbf{u}, z, \mathbf{y}) \alpha_{p,u}(t) \psi^{\text{sc}}(t, z, \mathbf{y}) dt d^n z d^m y \\ &= -(4\pi)^2 \int s_y^* [t + T_y - R_{p,z}(\bar{t}_{p,u}(t))/c - R_{p,y}(\bar{t}_{p,u}(t))/c] \\ &\quad \times R_{p,z}(\bar{t}_{p,u}(t)) R_{p,y}(\bar{t}_{p,u}(t)) \tilde{J}(\mathbf{p}, \mathbf{u}, z, \mathbf{y}) \alpha_{p,u}(t) \psi^{\text{sc}}(t, z, \mathbf{y}) dt d^n z d^m y, \end{aligned} \quad (40)$$

which has the form of a weighted matched filter. To obtain the second line of (40), we have used (12) to write the argument of s in a more symmetric form.

3.1.1. The point-spread function for the general case. We substitute equation (35) into equation (37), obtaining

$$I(\mathbf{p}, \mathbf{u}) = \int K(\mathbf{p}, \mathbf{u}; \mathbf{x}, \mathbf{v}) q_v(\mathbf{x}) d^3 x d^3 v, \quad (41)$$

where K , the point-spread function (PSF), is

$$\begin{aligned} K(\mathbf{p}, \mathbf{u}; \mathbf{x}, \mathbf{v}) &= \frac{1}{2\pi} \int e^{i\omega[\bar{t}_{p,u}(t) + T_y - R_{p,y}(\bar{t}_{p,u}(t))/c]} R_{p,z}(\bar{t}_{p,u}(t)) R_{p,y}(\bar{t}_{p,u}(t)) S_y^*(\omega) \alpha_{p,u} \\ &\quad \times \frac{J(\omega, \mathbf{p}, \mathbf{u}, z, \mathbf{y})}{(\omega)^2} d\omega \int \frac{(i\omega')^2 e^{-i\omega'(\bar{t}_{x,v}(t) + T_y - R_{x,y}(\bar{t}_{x,v}(t))/c)}}{R_{x,z}(\bar{t}_{x,v}(t)) R_{x,y}(\bar{t}_{x,v}(t))} \\ &\quad \times S_y(\omega') d\omega' dt d^n z d^m y. \end{aligned} \quad (42)$$

Since S_y is smooth, we can carry out a stationary phase reduction of (42) in the variables t and ω' . If we denote by ϕ the phase of (42), then the critical points are given by

$$0 = \frac{\partial \phi}{\partial t} = \omega \left[\frac{\partial \bar{t}_{p,u}}{\partial t} - \frac{\partial}{\partial t} \frac{R_{p,y}(\bar{t}_{p,u}(t))}{c} \right] - \omega' \left[\frac{\partial \bar{t}_{x,v}}{\partial t} - \frac{\partial}{\partial t} \frac{R_{x,y}(\bar{t}_{x,v}(t))}{c} \right] \quad (43)$$

$$0 = \frac{\partial \phi}{\partial \omega'} = \bar{t}_{x,v}(t) + T_y - \frac{R_{x,y}(\bar{t}_{x,v}(t))}{c} = t + T_y - \frac{R_{x,z}(\bar{t}_{x,v}(t))}{c} - \frac{R_{x,y}(\bar{t}_{x,v}(t))}{c}, \quad (44)$$

where in (44) we have used equation (12). These two conditions determine the critical values of ω' and t which give rise to the leading-order contributions to equation (42). We denote by $t_{x,v}^*$ the value of t determined by (44).

We rewrite equation (43) by differentiating (12) implicitly, obtaining

$$0 = 1 - \frac{\partial \bar{t}_{x,v}}{\partial t} - \widehat{\mathbf{R}}_{x,z}(\bar{t}_{x,v}(t)) \cdot \frac{\mathbf{v}}{c} \frac{\partial \bar{t}_{x,v}}{\partial t}, \quad (45)$$

which can be solved for $\partial \bar{t}_{x,v} / \partial t$ to obtain

$$\frac{\partial \bar{t}_{x,v}}{\partial t} = \frac{1}{1 + \widehat{\mathbf{R}}_{x,z}(\bar{t}_{x,v}(t)) \cdot \mathbf{v}/c}. \quad (46)$$

With (46) we see that the terms in brackets in (43) are of the form

$$\left[\frac{\partial \bar{t}_{x,v}}{\partial t} - \frac{\partial}{\partial t} \frac{R_{x,y}(\bar{t}_{x,v}(t))}{c} \right] = \frac{1 - \widehat{\mathbf{R}}_{x,y}(\bar{t}_{x,v}(t)) \cdot \mathbf{v}/c}{1 + \widehat{\mathbf{R}}_{x,z}(\bar{t}_{x,v}(t)) \cdot \mathbf{v}/c} = \alpha_{x,v}(t). \quad (47)$$

Thus we find that equation (43) implies that

$$\omega' = \frac{\alpha_{p,u}(t_{x,v}^*)}{\alpha_{x,v}(t_{x,v}^*)} \omega \quad (48)$$

and that, moreover, the determinant of the Hessian of the phase is

$$\begin{vmatrix} \frac{\partial^2 \phi}{\partial t^2} & \alpha_{x,v} \\ \alpha_{x,v} & 0 \end{vmatrix} = -\alpha_{x,v}^2. \quad (49)$$

The result of the stationary phase reduction of equation (42) is

$$\begin{aligned} K(\mathbf{p}, \mathbf{u}; \mathbf{x}, \mathbf{v}) &\sim \int e^{i\omega[\bar{t}_{p,u}(t_{x,v}^*) + T_y - R_{p,y}(\bar{t}_{p,u}(t_{x,v}^*))]/c} \frac{R_{p,z}(\bar{t}_{p,u}(t^*)) R_{p,y}(\bar{t}_{p,u}(t^*))}{R_{x,z}(\bar{t}_{x,v}(t^*)) R_{x,y}(\bar{t}_{x,v}(t^*))} S_y^*(\omega) \\ &\times S_y \left(\frac{\alpha_{p,u}(t_{x,v}^*)}{\alpha_{x,v}(t_{x,v}^*)} \omega \right) J(\omega, \mathbf{p}, \mathbf{u}, \mathbf{z}, \mathbf{y}) \frac{\alpha_{p,u}^3(t_{x,v}^*)}{\alpha_{x,v}^3(t_{x,v}^*)} d\omega d^n z d^m y. \end{aligned} \quad (50)$$

The quantity in square brackets in the phase of equation (50) can also be written as

$$\begin{aligned} \bar{t}_{p,u}(t_{x,v}^*) + T_y - \frac{R_{p,y}(\bar{t}_{p,u}(t_{x,v}^*))}{c} &= t_{x,v}^* + T_y - \frac{R_{p,z}(\bar{t}_{p,u}(t_{x,v}^*))}{c} - \frac{R_{p,y}(\bar{t}_{p,u}(t_{x,v}^*))}{c} \\ &= \frac{R_{x,z}(\bar{t}_{x,v}(t_{x,v}^*))}{c} + \frac{R_{x,y}(\bar{t}_{x,v}(t_{x,v}^*))}{c} - \frac{R_{p,z}(\bar{t}_{p,u}(t_{x,v}^*))}{c} - \frac{R_{p,y}(\bar{t}_{p,u}(t_{x,v}^*))}{c} + T_y, \end{aligned} \quad (51)$$

where in the first line we have used definition (12) of \bar{t} and in the second line definition (44) of t^* .

We write equation (50) as

$$\begin{aligned} K(\mathbf{p}, \mathbf{u}; \mathbf{x}, \mathbf{v}) &\sim \int e^{-i\omega \Delta \tau_{y,z}(\mathbf{x}, \mathbf{p}, \mathbf{u}, \mathbf{v})} S_y^*(\omega) S_y \left(\frac{\alpha_{p,u}}{\alpha_{x,v}} \omega \right) \\ &\times \mathcal{R}(\mathbf{x}, \mathbf{y}, \mathbf{z}, \mathbf{p}, \mathbf{u}, \mathbf{v}) J(\omega, \mathbf{p}, \mathbf{u}, \mathbf{z}, \mathbf{y}) \frac{\alpha_{p,u}^3}{\alpha_{x,v}^3} d\omega d^n z d^m y, \end{aligned} \quad (52)$$

where $k = \omega/c$ and where

$$\begin{aligned} c \Delta \tau_{y,z}(\mathbf{x}, \mathbf{p}, \mathbf{u}, \mathbf{v}) &= [R_{p,z}(\bar{t}_{p,u}(t_{x,v}^*)) + R_{p,y}(\bar{t}_{p,u}(t_{x,v}^*))] \\ &- [R_{x,z}(\bar{t}_{x,v}(t_{x,v}^*)) + R_{x,y}(\bar{t}_{x,v}(t_{x,v}^*))] + c T_y \end{aligned} \quad (53)$$

and

$$\mathcal{R}(\mathbf{x}, \mathbf{y}, \mathbf{z}, \mathbf{p}, \mathbf{u}, \mathbf{v}) = \frac{R_{p,z}(\bar{t}_{p,u}(t^*)) R_{p,y}(\bar{t}_{p,u}(t^*))}{R_{x,z}(\bar{t}_{x,v}(t^*)) R_{x,y}(\bar{t}_{x,v}(t^*))}. \quad (54)$$

3.1.2. Relation between point-spread function and ambiguity function in the general case.

In equation (52) we use the definition of the inverse Fourier transform

$$S_y(\omega) = \int e^{i\omega t} s_y(t) dt, \quad (55)$$

which, in the case when $J = \tilde{J}\omega^2$ with \tilde{J} independent of ω , converts (52) to

$$\begin{aligned}
 K(\mathbf{p}, \mathbf{u}; \mathbf{x}, \mathbf{v}) &= \int \left(-i\omega \frac{\alpha_{p,u}}{\alpha_{x,v}}\right) e^{-i\omega \Delta\tau_{y,z}} S_y^*(\omega) \int \left(i\omega \frac{\alpha_{p,u}}{\alpha_{x,v}}\right) \exp\left(i \frac{\alpha_{p,u}}{\alpha_{x,v}} \omega t\right) s_y(t) dt \\
 &\quad \times \mathcal{R}(\mathbf{x}, \mathbf{y}, \mathbf{z}, \mathbf{p}, \mathbf{u}, \mathbf{v}) \tilde{J}(\mathbf{p}, \mathbf{u}, \mathbf{z}, \mathbf{y}) \frac{\alpha_{p,u}}{\alpha_{x,v}} d\omega d^n z d^m y \\
 &\sim \int \dot{s}_y^* \left(\frac{\alpha_{p,u}}{\alpha_{x,v}} t - \Delta\tau_{y,z}(\mathbf{x}, \mathbf{p}, \mathbf{u}, \mathbf{v})\right) s_y(t) dt \\
 &\quad \times \mathcal{R}(\mathbf{x}, \mathbf{y}, \mathbf{z}, \mathbf{p}, \mathbf{u}, \mathbf{v}) \tilde{J}(\mathbf{p}, \mathbf{u}, \mathbf{z}, \mathbf{y}) \frac{\alpha_{p,u}}{\alpha_{x,v}} d^n z d^m y.
 \end{aligned} \tag{56}$$

Equation (56) can be written as

$$\boxed{K(\mathbf{p}, \mathbf{u}; \mathbf{x}, \mathbf{v}) \sim \int \mathcal{A}_y \left(\frac{\alpha_{p,u}}{\alpha_{x,v}}, \Delta\tau_{y,z}(\mathbf{x}, \mathbf{p}, \mathbf{u}, \mathbf{v})\right) \mathcal{R}(\mathbf{x}, \mathbf{y}, \mathbf{z}, \mathbf{p}, \mathbf{u}, \mathbf{v}) \frac{\alpha_{p,u}}{\alpha_{x,v}} \tilde{J} d^n z d^m y,} \tag{57}$$

where \mathcal{A}_y is the wideband radar ambiguity function [17] for the waveform \dot{s} , defined by

$$\mathcal{A}_y(\sigma, \tau) = \int \dot{s}_y^*(\sigma t - \tau) \dot{s}_y(t) dt. \tag{58}$$

Equation (57) is a general form appropriate to any target environment and any finite-duration interrogating waveform.

For a narrowband waveform (20), the ambiguity function is

$$\mathcal{A}_y(\sigma, \tau) = \omega_y^2 \int \tilde{s}_y^*(\sigma t - \tau) \tilde{s}_y(t) e^{i\tilde{\omega}t} e^{-i\omega_y \tau} dt, \tag{59}$$

where $\tilde{\omega} = \omega_y(\sigma - 1)$. Since $\tilde{s}_y(t)$ is slowly varying, $\mathcal{A}_y(\sigma, \tau) \approx \omega_y^2 \mathcal{A}_y(\tilde{\omega}, \tau)$, where

$$\mathcal{A}_y(\tilde{\omega}, \tau) = e^{-i\omega_y \tau} \int \tilde{s}_y^*(t - \tau) \tilde{s}_y(t) e^{i\tilde{\omega}t} dt. \tag{60}$$

In this narrowband case, the point-spread function of equation (57) can similarly be approximated by

$$\boxed{K_{\text{NB}}(\mathbf{p}, \mathbf{u}; \mathbf{x}, \mathbf{v}) \sim \int \omega_y^2 \mathcal{A}_y \left(\omega_y \left[\frac{\alpha_{p,u}}{\alpha_{x,v}} - 1\right], \Delta\tau_{y,z}\right) \mathcal{R}(\mathbf{x}, \mathbf{y}, \mathbf{z}, \mathbf{p}, \mathbf{u}, \mathbf{v}) \frac{\alpha_{p,u}}{\alpha_{x,v}} \tilde{J} d^n z d^m y,} \tag{61}$$

where $\Delta\tau_{y,z}$ is given by (53).

3.2. Imaging in the slow-mover case

In the slow-mover case, we write equation (19) as

$$\psi_s^{\text{sc}}(t, \mathbf{z}, \mathbf{y}) = - \int \frac{(i\omega')^2 e^{-i\omega'[\alpha_{x,v}(t-R_{x,z}(0)/c) - R_{x,y}(0)/c + T_y]}}{2^5 \pi^3 R_{x,z}(0) R_{x,y}(0)} S_y(\omega') d\omega' q_v(\mathbf{x}') d^3 x d^3 v. \tag{62}$$

The imaging formula in the slow-mover case is

$$I(\mathbf{p}, \mathbf{u}) = \int e^{i\omega[\alpha_{p,u}(t-R_{p,z}(0)/c) - R_{p,y}(0)/c + T_y]} Q(\omega, \mathbf{p}, \mathbf{u}, \mathbf{y}, \mathbf{z}) \psi_s^{\text{sc}}(t, \mathbf{z}, \mathbf{y}) d\omega dt d^3 y d^3 z. \tag{63}$$

The corresponding point-spread function is

$$K^s(\mathbf{p}, \mathbf{u}; \mathbf{x}, \mathbf{v}) = \frac{1}{2\pi} \int e^{i\omega[\alpha_{p,u}(t-R_{p,z}(0)/c)-R_{p,y}(0)/c+T_y]} e^{-i\omega'[\alpha_{x,v}(t-R_{x,z}(0)/c)-R_{x,y}(0)/c+T_y]} \\ \times S_y^*(\omega) S_y(\omega') \mathcal{R} J \alpha_{p,u} \frac{\omega^2}{\omega'^2} d\omega d\omega' dt d^n z d^m y. \quad (64)$$

In (64), we apply the method of stationary phase in the t and ω' integrals. The critical set is

$$0 = \alpha_{p,u}\omega - \alpha_{x,v}\omega' \\ 0 = \alpha_{x,v}(t - R_{x,z}(0)/c) - R_{x,y}(0)/c + T_y \quad (65)$$

and the Hessian of the phase is $-\alpha_{x,v}^2$. The leading-order contribution to (64) is thus

$$K^s(\mathbf{p}, \mathbf{u}; \mathbf{x}, \mathbf{v}) \sim \int \exp\left(ik\left[\alpha_{p,u}\left(\frac{R_{x,y}(0) - cT_y}{\alpha_{x,v}} + R_{x,z}(0) - R_{p,z}(0)\right) - R_{p,y}(0) + cT_y\right]\right) \\ \times S_y^*\left(\omega \frac{\alpha_{p,u}}{\alpha_{x,v}}\right) S_y(\omega) \mathcal{R} J \frac{\alpha_{p,u}^3}{\alpha_{x,v}^3} d\omega d^n z d^m y, \quad (66)$$

where $k = \omega/c$, or, in terms of the ambiguity function,

$$K^s(\mathbf{p}, \mathbf{u}; \mathbf{x}, \mathbf{v}) \sim \int \mathcal{A}\left(\frac{\alpha_{p,u}}{\alpha_{x,v}}, \Delta\tau_{y,z}^s(\mathbf{x}, \mathbf{p}, \mathbf{u}, \mathbf{v})\right) \mathcal{R}(\mathbf{x}, \mathbf{y}, z, \mathbf{p}, \mathbf{u}, \mathbf{v}) \tilde{J} \frac{\alpha_{p,u}}{\alpha_{x,v}} d^n z d^m y \quad (67)$$

under the assumption that $\tilde{J} = J/\omega^2$ is independent of ω . We note that the delay (second) argument of the ambiguity function can be written as

$$\Delta\tau_{y,z}^s = \alpha_{p,u} \frac{R_{x,z}(0) - R_{p,z}(0)}{c} + \left[\frac{\alpha_{p,u}}{\alpha_{x,v}} \left(\frac{R_{x,y}(0)}{c} - T_y\right) - \frac{R_{p,y}(0)}{c} + T_y\right] \\ = \alpha_{p,u} \frac{R_{x,z}(0) - R_{p,z}(0)}{c} + \left(\frac{\alpha_{p,u}}{\alpha_{x,v}} - 1\right) \frac{R_{x,y}(0)}{c} + \left(\frac{R_{x,y}(0)}{c} - \frac{R_{p,y}(0)}{c}\right) \\ - \left(\frac{\alpha_{p,u}}{\alpha_{x,v}} - 1\right) T_y \\ = \alpha_{p,u} \frac{R_{x,z}(0) - R_{p,z}(0)}{c} + \frac{R_{x,y}(0) - R_{p,y}(0)}{c} + \left(\frac{\alpha_{p,u}}{\alpha_{x,v}} - 1\right) \left(\frac{R_{x,y}(0)}{c} - T_y\right) \\ \approx \frac{\mathbf{x} - \mathbf{p}}{c} \cdot (\alpha_{p,u} \hat{\mathbf{R}}_{x,z}(0) + \hat{\mathbf{R}}_{x,y}(0)) + \frac{\mathbf{u} - \mathbf{v}}{c} \cdot (\hat{\mathbf{R}}_{x,y}(0) + \hat{\mathbf{R}}_{x,z}(0)) \left(\frac{R_{x,y}(0)}{c} - T_y\right), \quad (68)$$

where in the second line we have added and subtracted $R_{x,y}(0)/c$. If the target scene is not too large, the transmitters can be activated at times $-T_y$ chosen so that $R_{x,y}(0)/c - T_y$ is negligible.

3.3. Imaging in the slow-mover, narrow-band case

Under the slow-mover, narrow-band assumptions, the data (21) can be written as

$$\psi_N^{sc}(t, z, \mathbf{y}) \approx - \int \frac{\omega_y^2 e^{i\varphi_{x,v}} e^{-i\omega_y \alpha_{x,v} t}}{(4\pi)^2 R_{x,z}(0) R_{x,y}(0)} \tilde{s}_y(t + T_y - (R_{x,z}(0) + R_{x,y}(0))/c) q_v(\mathbf{x}) d^3 x d^3 v. \quad (69)$$

The corresponding imaging operation (from equation (40)) is

$$I_{\text{cl}}(\mathbf{p}, \mathbf{u}) = -(4\pi)^2 \int e^{-i\varphi_{p,u}} e^{i\omega_y \alpha_{p,u} t} R_{p,z}(0) R_{p,y}(0) \tilde{s}_y^*(t + T_y - (R_{p,z}(0) + R_{p,y}(0))/c) \psi_N^{\text{sc}}(t, \mathbf{z}, \mathbf{y}) \tilde{J} dt d^n z d^m y. \quad (70)$$

The operation (70) amounts to geometry-corrected, phase-corrected matched filtering with a time-delayed, Doppler-shifted version of the transmitted waveform, where the Doppler shift is defined in terms of (23).

Under the assumption that \tilde{J} is independent of ω , the point-spread function is

$$K_{\text{cl}}(\mathbf{p}, \mathbf{u}; \mathbf{x}, \mathbf{v}) = \int \omega_y^2 \tilde{s}_y^*(t + T_y - (R_{p,z}(0) + R_{p,y}(0))/c) e^{i\omega_y [\beta_{p,u} - \beta_{x,v}] t} \times \tilde{s}_y(t + T_y - (R_{x,z}(0) + R_{x,y}(0))/c) \exp(i[\varphi_{x,v} - \varphi_{p,u}]) \times \frac{R_{p,z}(0) R_{p,y}(0)}{R_{x,z}(0) R_{x,y}(0)} \tilde{J} dt d^n z d^m y. \quad (71)$$

In the second exponential of equation (71) we use (22) to write

$$\begin{aligned} \varphi_{x,v} - \varphi_{p,u} &= k_y [R_{x,y}(0) - T_y + (1 + \beta_{x,v}) R_{x,z}(0)] \\ &\quad - k_y [R_{p,y}(0) - T_y + (1 + \beta_{p,u}) R_{p,z}(0)] \\ &= k_y [-c \Delta \tau_{y,z}^{\text{cl}} + \beta_{x,v} R_{x,z}(0) - \beta_{p,u} R_{p,z}(0)], \end{aligned} \quad (72)$$

where

$$c \Delta \tau_{y,z}^{\text{cl}} = [R_{p,z}(0) + R_{p,y}(0)] - [R_{x,z}(0) + R_{x,y}(0)] \quad (73)$$

is the difference in bistatic ranges for the points \mathbf{x} and \mathbf{p} . If in (71) we make the change of variables $t' = t + T_y - (R_{x,z}(0) + R_{x,y}(0))/c$ and use (60), then we obtain

$$K_{\text{cl}}(\mathbf{p}, \mathbf{u}; \mathbf{x}, \mathbf{v}) = \int \omega_y^2 A(\omega_y [\beta_{p,u} - \beta_{x,v}], \Delta \tau_{y,z}^{\text{cl}}) \times \exp(i\omega_y [\beta_{p,u} - \beta_{x,v}] [R_{x,y}(0)/c - T_y]) \times \exp(-ik_y \beta_{p,u} [R_{x,z}(0) - R_{p,z}(0)]) \frac{R_{p,z}(0) R_{p,y}(0)}{R_{x,z}(0) R_{x,y}(0)} \tilde{J} d^n z d^m y. \quad (74)$$

We note that the narrowband ambiguity function of (74) depends on the difference of bistatic ranges (73) and on the difference between the velocity projections onto the bistatic bisectors: $\beta_{p,u} - \beta_{x,v} = (\hat{\mathbf{R}}_{x,y}(0) + \hat{\mathbf{R}}_{x,z}(0)) \cdot \mathbf{v}/c - (\hat{\mathbf{R}}_{p,y}(0) + \hat{\mathbf{R}}_{p,z}(0)) \cdot \mathbf{u}/c$.

For the case of a single transmitter and single receiver (a case for which $\tilde{J} = 1$) and a point target (which enables us to choose T_y so that the exponential in the second line of (74) vanishes), and leaving aside the magnitude and phase corrections, (74) reduces to a coordinate-independent version of the ambiguity function of [18].

3.4. Imaging in the far-field case

3.4.1. *Imaging in the far-field wideband case.* Our filtered-adjoint imaging formula reduces to

$$I_{\infty}(\mathbf{p}, \mathbf{u}) = \int e^{i\omega [\alpha_u(t - |z|/c + \hat{\mathbf{z}} \cdot \mathbf{p}/c) - |y|/c + \hat{\mathbf{y}} \cdot \mathbf{p}/c + T_y]} \times Q_{\infty}(\omega, \mathbf{p}, \mathbf{u}, \mathbf{z}, \mathbf{y}) d\omega \psi^{\text{sc}}(t, \mathbf{z}, \mathbf{y}) dt d^n z d^m y, \quad (75)$$

where we take the filter to be

$$Q_{\infty}(\omega, \mathbf{p}, \mathbf{u}, \mathbf{z}, \mathbf{y}) = -(4\pi)^2 \omega^{-2} |z| |y| S_y^*(\omega) J(\omega, \mathbf{p}, \mathbf{u}, \mathbf{z}, \mathbf{y}) \alpha_u. \quad (76)$$

To determine the point-spread function, we substitute (29) into (75) to obtain

$$\begin{aligned}
 I_\infty(\mathbf{p}, \mathbf{u}) &= \int \exp(i\omega[\alpha_u(t - |\mathbf{z}|/c + \hat{\mathbf{z}} \cdot \mathbf{p}/c) - |\mathbf{y}|/c + \hat{\mathbf{y}} \cdot \mathbf{p}/c + T_y]) Q_\infty(\omega, \mathbf{p}, \mathbf{u}, \mathbf{z}, \mathbf{y}) \\
 &\quad \times \int \exp(-i\omega'[\alpha_v(t - |\mathbf{z}|/c + \hat{\mathbf{z}} \cdot \mathbf{x}/c) - |\mathbf{y}|/c + \hat{\mathbf{y}} \cdot \mathbf{x}/c + T_y]) \\
 &\quad \times \frac{\omega'^2 S_y(\omega')}{2^5 \pi^3 |\mathbf{z}| |\mathbf{y}|} d\omega' d\omega q_v(\mathbf{x}) d^3x d^3v dt d^n z d^m y.
 \end{aligned} \tag{77}$$

For smooth S_y , we can apply the method of stationary phase to the t and ω' integrations in (77). The critical conditions are

$$\begin{aligned}
 0 &= \omega\alpha_u - \omega'\alpha_v \\
 0 &= \alpha_v(t - |\mathbf{z}|/c + \hat{\mathbf{z}} \cdot \mathbf{x}/c) - |\mathbf{y}|/c + \hat{\mathbf{y}} \cdot \mathbf{x}/c + T_y
 \end{aligned} \tag{78}$$

and the Hessian of the phase is α_v . This converts the kernel of (77) into

$$K_\infty(\mathbf{p}, \mathbf{u}; \mathbf{x}, \mathbf{v}) \sim \int \exp(-i\omega \Delta\tau_{y,z}^f) S_y^*(\omega) S_y\left(\frac{\omega\alpha_u}{\alpha_{x,v}}\right) \frac{J\alpha_u^3}{\alpha_v^3} d\omega d^n z d^m y, \tag{79}$$

where $\Delta\tau_f$ is defined by

$$\begin{aligned}
 c\Delta\tau_{y,z}^f &= \alpha_u \left(|\mathbf{z}| - \hat{\mathbf{z}} \cdot \mathbf{x} + \frac{|\mathbf{y}| - \hat{\mathbf{y}} \cdot \mathbf{x} - cT_y}{\alpha_v} - |\mathbf{z}| + \hat{\mathbf{z}} \cdot \mathbf{p} \right) - |\mathbf{y}| + \hat{\mathbf{y}} \cdot \mathbf{p} + cT_y \\
 &= \alpha_u \hat{\mathbf{z}} \cdot (\mathbf{p} - \mathbf{x}) + \left(\frac{\alpha_u}{\alpha_v} - 1 \right) (|\mathbf{y}| - cT_y) - \hat{\mathbf{y}} \cdot \left(\frac{\alpha_u}{\alpha_v} \mathbf{x} - \mathbf{p} \right) \\
 &= \alpha_u \hat{\mathbf{z}} \cdot (\mathbf{p} - \mathbf{x}) + \left(\frac{\alpha_u}{\alpha_v} - 1 \right) (|\mathbf{y}| - cT_y) - \hat{\mathbf{y}} \cdot \left(\frac{\alpha_u}{\alpha_v} - 1 \right) \mathbf{x} - \hat{\mathbf{y}} \cdot (\mathbf{x} - \mathbf{p}) \\
 &= (\alpha_u \hat{\mathbf{z}} + \hat{\mathbf{y}}) \cdot (\mathbf{p} - \mathbf{x}) + \left(\frac{\alpha_u}{\alpha_v} - 1 \right) (|\mathbf{y}| - cT_y) - \left(\frac{\alpha_u}{\alpha_v} - 1 \right) \hat{\mathbf{y}} \cdot \mathbf{x} \\
 &\approx (\alpha_u \hat{\mathbf{z}} + \hat{\mathbf{y}}) \cdot (\mathbf{p} - \mathbf{x}) + \left(\frac{\mathbf{u} - \mathbf{v}}{c} \right) \cdot (\hat{\mathbf{y}} + \hat{\mathbf{z}}) \hat{\mathbf{y}} \cdot \mathbf{x},
 \end{aligned} \tag{80}$$

where we have made the choice $T_y = |\mathbf{y}|/c$ in the last line and where we have used (28) to write

$$\frac{\alpha_u}{\alpha_v} \approx 1 - (\mathbf{u} - \mathbf{v}) \cdot (\hat{\mathbf{y}} + \hat{\mathbf{z}})/c. \tag{81}$$

To write (79) in terms of the ambiguity function, we assume that $\tilde{J} = J/\omega^2$ is independent of ω and use (55) to obtain

$$K_\infty(\mathbf{p}, \mathbf{u}; \mathbf{x}, \mathbf{v}) \sim \int \hat{s}_y^* \left(\frac{\alpha_u}{\alpha_v} t - \Delta\tau_{y,z}^f, \mathbf{y} \right) \hat{s}_y(t) \tilde{J} \frac{\alpha_u}{\alpha_v} dt d^n z d^m y. \tag{82}$$

Using (58), we obtain for the wideband far-field point-spread function

$$\boxed{K_\infty(\mathbf{p}, \mathbf{u}; \mathbf{x}, \mathbf{v}) \sim \int \mathcal{A}_y \left(\frac{\alpha_u}{\alpha_v}, \Delta\tau_{y,z}^f \right) \tilde{J}(\mathbf{p}, \mathbf{u}, \mathbf{z}, \mathbf{y}) \frac{\alpha_u}{\alpha_v} d^n z d^m y.} \tag{83}$$

We note that (83) no longer involves a ratio of ranges, because now the corresponding ranges are referenced to the scene center and not to the individual point \mathbf{x} or \mathbf{p} .

3.4.2. *Imaging in the far-field, narrowband case.* In the case of a narrowband waveform (20), we use the matched-filter interpretation of the imaging formula

$$I_\infty(\mathbf{p}, \mathbf{u}) = \frac{(4\pi)^2 |\mathbf{z}| |\mathbf{y}|}{-\omega_y^2} \int e^{-i\tilde{\varphi}_{p,u}} e^{+i\omega_y(1+\beta_u)t'} \tilde{s}_y^*(t' + (\hat{\mathbf{z}} + \hat{\mathbf{y}}) \cdot \mathbf{p}/c) \times \psi^{sc}(t', \mathbf{z}, \mathbf{y}) J(\omega_y, \mathbf{p}, \mathbf{u}, \mathbf{z}, \mathbf{y}) dt' d^n z d^m y. \tag{84}$$

Inserting (31) into (84), we obtain for the point-spread function

$$K_\infty^{(NB)}(\mathbf{p}, \mathbf{u}; \mathbf{x}, \mathbf{v}) = \omega_y^2 \int e^{i(\tilde{\varphi}_{x,v} - \tilde{\varphi}_{p,u})} e^{i\omega_y(\beta_u - \beta_v)t'} \tilde{s}_y^*(t' + (\hat{\mathbf{z}} + \hat{\mathbf{y}}) \cdot \mathbf{p}/c) \times \tilde{s}_y(t' + (\hat{\mathbf{z}} + \hat{\mathbf{y}}) \cdot \mathbf{x}/c) \tilde{J} dt' d^n z d^m y. \tag{85}$$

In the first exponential of equation (85) we use (32),

$$\begin{aligned} \tilde{\varphi}_{x,v} - \tilde{\varphi}_{p,u} &= \frac{\omega_y}{c} [(1 + \beta_u)\hat{\mathbf{z}} + \hat{\mathbf{y}}] \cdot \mathbf{p} - [(1 + \beta_v)\hat{\mathbf{z}} + \hat{\mathbf{y}}] \cdot \mathbf{x} \\ &= k_y [(\hat{\mathbf{z}} + \hat{\mathbf{y}}) \cdot (\mathbf{p} - \mathbf{x}) + \hat{\mathbf{z}} \cdot (\beta_u \mathbf{p} - \beta_v \mathbf{x})], \end{aligned} \tag{86}$$

where $k_y = \omega_y/c$.

In (85) we also make the change of variables $t = t' + (\hat{\mathbf{z}} + \hat{\mathbf{y}}) \cdot \mathbf{x}/c$, use (60) and $\beta_v = (\hat{\mathbf{y}} + \hat{\mathbf{z}}) \cdot \mathbf{v}/c$ to obtain

$$K_\infty^{(NB)}(\mathbf{p}, \mathbf{u}; \mathbf{x}, \mathbf{v}) = \int \omega_y^2 A(k_y(\hat{\mathbf{y}} + \hat{\mathbf{z}}) \cdot (\mathbf{u} - \mathbf{v}), (\hat{\mathbf{z}} + \hat{\mathbf{y}}) \cdot (\mathbf{x} - \mathbf{p})/c) \times \exp[i(\tilde{\varphi}_{x,v} - \tilde{\varphi}_{p,u})] \exp(-ik_y(\beta_u - \beta_v)(\hat{\mathbf{z}} + \hat{\mathbf{y}}) \cdot \mathbf{x}) \tilde{J} d^n z d^m y,$$

(87)

Here we see clearly the dependence on the familiar bistatic bisector $\hat{\mathbf{y}} + \hat{\mathbf{z}}$.

4. Reduction to familiar special cases

4.1. Range-Doppler imaging

In classical range-Doppler imaging, the range and velocity of a moving target are estimated from measurements made by a single transmitter and coincident receiver. Thus we take $\mathbf{z} = \mathbf{y}$, $\tilde{J} = 1$, and remove the integrals in (87) or (74) to show that the point-spread function is simply proportional to the ambiguity function. In particular, for the case of a slowly-moving distant target, (87) reduces to the familiar result

$$K_{RD}^{(NB)}(\mathbf{p}, \mathbf{u}; \mathbf{x}, \mathbf{v}) \propto A_y \left(2 \frac{\omega_c(\mathbf{u} - \mathbf{v}) \cdot \hat{\mathbf{y}}}{c}, 2 \frac{(\mathbf{p} - \mathbf{x}) \cdot \hat{\mathbf{y}}}{c} \right). \tag{88}$$

We see that only range and down-range velocity information is obtained.

4.1.1. *Range-Doppler imaging of a rotating target.* If the target is rotating about a point, then we can use the connection between position and velocity to form a target image. We choose the center of rotation as the origin of coordinates. In this case, a scatterer at \mathbf{x} moves as $q(\mathcal{O}(t)\mathbf{x})$, where \mathcal{O} denotes an orthogonal matrix. This is not linear motion, but we can still apply our results by approximating the motion as linear over a small angle.

In particular, we write $\mathcal{O}(t) = \mathcal{O}(0) + t\dot{\mathcal{O}}(0)$, and assume that $\mathcal{O}(0)$ is the identity operator. In this case, the velocity at the point \mathbf{x} is $\dot{\mathcal{O}}(0)\mathbf{x}$, so in our notation, the phase-space distribution is $q_v(\mathbf{x}) = q_{\dot{\mathcal{O}}(0)\mathbf{x}}(\mathbf{x})$.

For the case of two-dimensional imaging, we take $\hat{\mathbf{y}} = (1, 0)$, and \mathcal{O} is given by

$$\mathcal{O}(t) = \begin{bmatrix} \cos \omega t & \sin \omega t \\ -\sin \omega t & \cos \omega t \end{bmatrix}, \quad \dot{\mathcal{O}}(0) = \dot{\omega} \begin{bmatrix} 0 & 1 \\ -1 & 0 \end{bmatrix}, \quad (89)$$

so (88) becomes

$$K_{\text{RD}}^{(\text{NB})}(\mathbf{p}, \mathbf{u}; \mathbf{x}, \mathbf{v}) \propto A_y \left(2 \frac{\omega_c(u_1 - v_1)}{c}, 2 \frac{(p_1 - x_1)}{c} \right) \propto A_y \left(2 \frac{\omega_c \dot{\omega} (p_2 - x_2)}{c}, 2 \frac{(p_1 - x_1)}{c} \right). \quad (90)$$

Thus we have the familiar result that the delay provides the down-range target components while the Doppler shift provides the cross-range components. Note that even though the velocity $v_1 = \dot{\omega} x_1$ can be estimated from the radar measurements, the cross-range spatial components are distorted by the unknown angular velocity $\dot{\omega}$.

The PSF depends on only two variables, which implies that the image obtained is an approximation to $\int q(x_1, x_2, x_3) dx_3$.

4.2. Inverse synthetic-aperture radar (ISAR)

Modern ISAR methods do not actually require Doppler-shift measurements at all. Rather, the technique depends on the target's rotational motion to establish a pseudo-array of distributed receivers. To show how ISAR follows from the results of this paper, we fix the coordinate system to the rotating target. Succeeding pulses of a pulse train are transmitted from and received at positions $\mathbf{z} = \mathbf{y}$ that rotate around the target as $\hat{\mathbf{y}} = \hat{\mathbf{y}}(\theta)$. The pulses typically used in ISAR are high range-resolution (HRR) ones, so that each pulse yields a ridge-like ambiguity function $A_y(\nu, \tau) = \bar{A}_y(\tau)$, with $\bar{A}_y(\tau)$ sharply peaked around $\tau = 0$. Equation (87) reduces to

$$K_{\text{ISAR}}^{(\text{NB})}(\mathbf{p}, \mathbf{u}; \mathbf{x}, \mathbf{v}) = -\omega_0^2 \int \bar{A}_y \left(2 \frac{(\mathbf{p} - \mathbf{x}) \cdot \hat{\mathbf{y}}(\theta)}{c} \right) \tilde{J}|\mathbf{y}| d\theta, \quad (91)$$

where we have written $\omega_y = \omega_0$ because the pulses typically have the same center frequency.

Note that the set of all points \mathbf{p} such that $(\mathbf{p} - \mathbf{x}) \cdot \hat{\mathbf{y}}(\theta) = 0$ forms a plane through \mathbf{x} with normal $\hat{\mathbf{y}}(\theta)$. Consequently, since $\bar{A}_y(\tau)$ is sharply peaked around $\tau = 0$, the support of the integral in (91) is a collection of planes, one for each pulse in the pulse train, and ISAR imaging is seen to be based on backprojection.

Because knowledge of $\hat{\mathbf{y}}(\theta)$ is needed, ISAR depends on knowledge of the rotational motion; it is typically assumed to be uniform, and the rotation rate $\dot{\omega}$ must be determined by other means.

Useful information can be obtained from the PSF as follows. If we approximate the HRR ambiguity function by

$$\bar{A}(\tau) = \int_B \exp(i\omega\tau) d\omega, \quad (92)$$

where B denotes the bandwidth, then we find that (91) becomes

$$\begin{aligned} K_{\text{ISAR}}^{(\text{NB})}(\mathbf{p}, \mathbf{u}; \mathbf{x}, \mathbf{v}) &\propto \int_B \int \exp(i2\omega(\mathbf{p} - \mathbf{x}) \cdot \hat{\mathbf{y}}(\theta)/c) \tilde{J}|\mathbf{y}| d\omega d\theta \\ &\propto \int \exp(i(\mathbf{p} - \mathbf{x}) \cdot \boldsymbol{\xi}) \left| \frac{\partial(\omega, \theta)}{\partial \boldsymbol{\xi}} \right| \tilde{J}|\mathbf{y}| d^2 \boldsymbol{\xi}, \end{aligned} \quad (93)$$

where we have made the change of variables $(\omega, \theta) \mapsto \boldsymbol{\xi} = 2\omega\hat{\mathbf{y}}(\theta)/c$. This is a two-dimensional change of variables, so again the PSF depends on only two variables, and the image involves a projection of the third variable onto the other two.

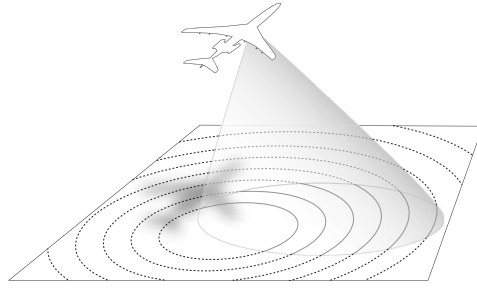


Figure 3. For SAR, we consider a stationary scene and a sensor that (in the start–stop approximation) does not move as it transmits and receives each pulse. Between pulses, the sensor moves to a different location along the flight path.

The factor J of (87) should be chosen to be the Jacobian $|\partial\xi/(\omega, \theta)| = \omega^2 \tilde{J}(\theta)$ (i.e., the reciprocal of the factor $|\partial(\omega, \theta)/\partial\xi|$ appearing in (91)). The narrowband approximation uses $\omega \approx \omega_0$, so the result is

$$K_{\text{ISAR}}^{(\text{NB})}(\mathbf{p}, \mathbf{u}; \mathbf{x}, \mathbf{v}) \propto \int_{\Omega} \exp(i(\mathbf{p} - \mathbf{x}) \cdot \boldsymbol{\xi}) \, d^2\xi, \tag{94}$$

where Ω denotes the region in $\boldsymbol{\xi}$ -space for which we have data. This region Ω is a sector of an annulus with width $2B$ and angular extent corresponding to the angular aperture. The form (94) is useful for determining resolution of the imaging system. In particular, the Fourier components of the target that are visible correspond to the values of $\boldsymbol{\xi}$ that are obtained as ω ranges over the frequency band of the radar system and θ ranges over the angles of view.

4.3. Synthetic-aperture radar (SAR)

SAR also uses high range-resolution pulses, transmitted and received at locations along the flight path $\mathbf{y} = \mathbf{y}(\zeta)$, where ζ denotes the flight path parameter (see figure 3). For a stationary scene, $\mathbf{u} = \mathbf{v} = \mathbf{0}$, which implies that $\beta_u = \beta_v = 0$. In this case, (74) reduces to

$$K_{\text{SAR}}^{(\text{NB})}(\mathbf{p}, 0; \mathbf{x}, 0) \propto \int \bar{A}_y \left(2 \frac{(R_{\mathbf{p}, \mathbf{y}(\zeta)}(0) - R_{\mathbf{x}, \mathbf{y}(\zeta)}(0))}{c} \right) \frac{R_{\mathbf{p}, \mathbf{y}(\zeta)}^2(0)}{R_{\mathbf{x}, \mathbf{y}(\zeta)}^2(0)} \tilde{J} |\dot{\mathbf{y}}| \, d\zeta, \tag{95}$$

where again $\bar{A}_y(\tau)$ is sharply peaked around $\tau = 0$. Thus SAR imaging reduces to backprojection over circles $R_{\mathbf{p}, \mathbf{y}(\zeta)}(0) = R_{\mathbf{x}, \mathbf{y}(\zeta)}(0)$.

If we again approximate the HRR ambiguity function by (92), then we find that (95) becomes

$$\begin{aligned} K_{\text{SAR}}^{(\text{NB})}(\mathbf{p}, 0; \mathbf{x}, 0) &\propto \int \exp \left(i 2\omega \frac{R_{\mathbf{p}, \mathbf{y}(\zeta)}(0) - R_{\mathbf{x}, \mathbf{y}(\zeta)}(0)}{c} \right) \frac{R_{\mathbf{p}, \mathbf{y}(\zeta)}^2(0)}{R_{\mathbf{x}, \mathbf{y}(\zeta)}^2(0)} \tilde{J} |\dot{\mathbf{y}}| \, d\omega \\ &\propto \int \exp(i(\mathbf{p} - \mathbf{x}) \cdot \boldsymbol{\xi}) \frac{R_{\mathbf{p}, \mathbf{y}(\zeta)}^2(0)}{R_{\mathbf{x}, \mathbf{y}(\zeta)}^2(0)} \left| \frac{\partial(\omega, \zeta)}{\partial \boldsymbol{\xi}} \right| \tilde{J} |\dot{\mathbf{y}}| \, d\xi, \end{aligned} \tag{96}$$

where we have made the Taylor expansion $R_{\mathbf{p}, \mathbf{y}(\zeta)}(0) - R_{\mathbf{x}, \mathbf{y}(\zeta)}(0) = (\mathbf{x} - \mathbf{p}) \cdot \hat{\mathbf{R}}_{\mathbf{p}, \mathbf{y}(\zeta)}(0) + \dots$ and the change of variables $(\omega, \zeta) \mapsto \boldsymbol{\xi} = 2\omega \hat{\mathbf{R}}_{\mathbf{p}, \mathbf{y}(\zeta)}(0)$. Again J should be chosen to be the reciprocal of the Jacobian $|\partial(\omega, \theta)/\partial\xi|$, and we note that the reciprocal $|\partial\xi/\partial(\omega, \theta)|$ is indeed of the form $\omega^2 \tilde{J}$, with \tilde{J} independent of ω .

Again the fact that the PSF depends on two variables gives rise to an image of a projected version of the target.

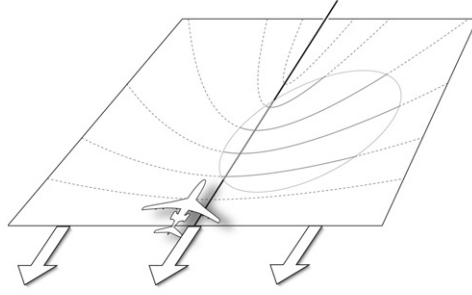


Figure 4. For Doppler SAR, we use a frame of reference in which the sensor is fixed and the plane below is moving with a uniform velocity.

4.4. Doppler SAR

Doppler SAR uses a high Doppler-resolution waveform, such as an approximation to the ideal single-frequency waveform $s(t) = \exp(-i\omega_0 t)$ transmitted from locations along the flight path $\mathbf{y} = \mathbf{y}(\zeta)$ (see figure 4). If we transform to the sensor frame of reference, then the entire scene is moving with velocity $\mathbf{u} = \mathbf{v} = -\dot{\mathbf{y}}(\zeta)$.

Although the stationary phase analysis of section 3.1.1 does not technically apply to a single-frequency waveform, it does apply to the time-limited waveforms that are used in practice. Consequently, the analysis of section 3.1.1 applies to a realizable system.

For a high Doppler-resolution waveform, $A_{\mathbf{y}}(\nu, \tau) = \bar{A}_{\mathbf{y}}(\nu)$, where $\bar{A}_{\mathbf{y}}(\nu)$ is sharply peaked around $\nu = 0$. In the monostatic case, (74) reduces to

$$\begin{aligned} K_{\text{HDR}}^{(\text{NB})}(\mathbf{p}, -\dot{\mathbf{y}}(\zeta); \mathbf{x}, -\dot{\mathbf{y}}(\zeta)) &\propto \int \bar{A}_{\mathbf{y}}(\omega_0[\beta_p(\zeta) - \beta_x(\zeta)]) \\ &\times \exp(i\omega_0[\beta_p(\zeta) - \beta_x(\zeta)][R_{x,y}(0) - T_y]) \\ &\times \exp(-ik_0\beta_p(\zeta)[R_{x,y}(0) - R_{p,y}(0)]) \frac{R_{p,y(\zeta)}^2(0)}{R_{x,y(\zeta)}^2(0)} \tilde{J} d\zeta, \end{aligned} \quad (97)$$

where from (23), $\beta_x(\zeta) \equiv \beta_{x,-\dot{\mathbf{y}}(\zeta)} = -2\widehat{\mathbf{R}}_{x,y(\zeta)}(0) \cdot \mathbf{v}/c = 2\widehat{\mathbf{R}}_{x,y(\zeta)}(0) \cdot \dot{\mathbf{y}}(\zeta)/c$. Again the imaging process reduces to backprojection over hyperbolas $\widehat{\mathbf{R}}_{p,y(\zeta)}(0) \cdot \dot{\mathbf{y}}(\zeta) = \widehat{\mathbf{R}}_{x,y(\zeta)}(0) \cdot \dot{\mathbf{y}}(\zeta)$.

If we again approximate the ridge-like ambiguity function by $\bar{A}(\nu) = \int \exp(i\nu t') dt'$, then (97) becomes

$$\begin{aligned} K_{\text{HDR}}^{(\text{NB})}(\mathbf{p}, -\dot{\mathbf{y}}(\zeta); \mathbf{x}, -\dot{\mathbf{y}}(\zeta)) &\propto \int \exp(it'\omega_0[\beta_p(\zeta) - \beta_x(\zeta)]) \\ &\times \exp(i\omega_0[\beta_p(\zeta) - \beta_x(\zeta)][R_{x,y}(0) - T_y]) \\ &\times \exp(-ik_0\beta_p(\zeta)[R_{x,y}(0) - R_{p,y}(0)]) \frac{R_{p,y(\zeta)}^2(0)}{R_{x,y(\zeta)}^2(0)} \tilde{J} dt' d\zeta \\ &\propto \int \exp(i(\mathbf{p} - \mathbf{x}) \cdot \boldsymbol{\xi}) \exp(i\omega_0[\beta_p(\zeta) - \beta_x(\zeta)][R_{x,y}(0) - T_y]) \\ &\times \exp(-ik_0\beta_p(\zeta)[R_{x,y}(0) - R_{p,y}(0)]) \frac{R_{p,y(\zeta)}^2(0)}{R_{x,y(\zeta)}^2(0)} \left| \frac{\partial(t', \zeta)}{\partial \boldsymbol{\xi}} \right| \tilde{J} d\boldsymbol{\xi}, \end{aligned} \quad (98)$$

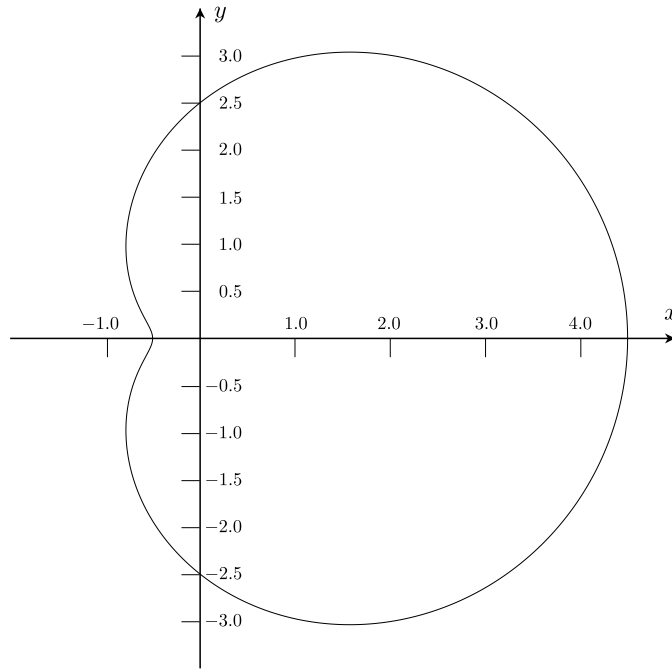


Figure 5. A limaçon of Pascal. The origin is located at the transmitter position y .

where we have made the Taylor expansion $\beta_p(\zeta) - \beta_x(\zeta) = (\mathbf{p} - \mathbf{x}) \cdot \nabla_p \beta_p(\zeta)$ and then made the change of variables $(t', \zeta) \mapsto \boldsymbol{\xi} = t' \omega_0 \nabla_p \beta_p(\zeta)$. We note that again J should be $|\partial \boldsymbol{\xi} / \partial (t', \zeta)| = \omega_0^2 \tilde{J}$, where \tilde{J} is independent of ω_0 . Again the image involves a projection.

4.5. SAR for other ridge-like ambiguity functions

In the above scenario, SAR reconstruction can be done with a sensor moving along the path $\mathbf{y} = \mathbf{y}(\zeta)$ while transmitting other waveforms. In particular, waveforms (such as chirps) can be used which produce a ridge-like ambiguity function along any line $v = \eta \tau$ in the delay-Doppler plane. Then (74) reduces to

$$\begin{aligned}
 K_\eta^{(\text{NB})}(\mathbf{p}, -\dot{\mathbf{y}}(\zeta); \mathbf{x}, -\dot{\mathbf{y}}(\zeta)) &\propto \int \bar{A}_y(\omega_0[\beta_p(\zeta) - \beta_x(\zeta)] - 2\eta(R_{p,y(\zeta)}(0) - R_{x,y(\zeta)}(0))/c) J \\
 &\times \exp(i\omega_0[\beta_p(\zeta) - \beta_x(\zeta)] [R_{x,y}(0) - T_y]) \\
 &\times \exp(-ik_0 \beta_p(\zeta) [R_{x,y}(0) - R_{p,y}(0)]) \frac{R_{p,y(\zeta)}^2(0)}{R_{x,y(\zeta)}^2(0)} d\zeta, \tag{99}
 \end{aligned}$$

which corresponds to backprojection over the planar curve $L_p(\zeta) = L_x(\zeta)$, where

$$L_p(\zeta) = -\omega_0 \hat{\mathbf{R}}_{p,y(\zeta)} \cdot \dot{\mathbf{y}}(\zeta) + \eta R_{p,y(\zeta)}(0). \tag{100}$$

The curve $L_p(\zeta)$ is the intersection of the imaging plane with a surface generated by rotating a limaçon of Pascal (figure 5) about the flight velocity vector. We note that for a slowly-moving sensor and a side-looking beam pattern, the curve obtained from the limaçon is almost indistinguishable from a circle.

If we approximate the ridge-like ambiguity function as $\overline{A}(v - \eta\tau) = \int \exp[i\omega(v - \eta\tau)] d\omega$, then (99) can be written as

$$\begin{aligned}
 K_\eta^{(NB)}(\mathbf{p}, \mathbf{u}; \mathbf{x}, \mathbf{v}) &\propto \int \exp(2\omega[L_p(\zeta) - L_x(\zeta)]/c) \tilde{J} \exp(i\omega_0[\beta_p(\zeta) - \beta_x(\zeta)][R_{x,y}(0) - T_y]) \\
 &\quad \times \exp(-ik_0\beta_p(\zeta)[R_{x,y}(0) - R_{p,y}(0)]) \frac{R_{p,y(\zeta)}^2(0)}{R_{x,y(\zeta)}^2(0)} d\omega d\zeta \\
 &\propto \int \exp([\mathbf{x} - \mathbf{p}] \cdot \boldsymbol{\xi}) \tilde{J} \exp(i\omega_0[\beta_p(\zeta) - \beta_x(\zeta)][R_{x,y}(0) - T_y]) \\
 &\quad \times \exp(-ik_0\beta_p(\zeta)[R_{x,y}(0) - R_{p,y}(0)]) \frac{R_{p,y(\zeta)}^2(0)}{R_{x,y(\zeta)}^2(0)} \left| \frac{\partial(\omega, \theta)}{\partial \boldsymbol{\xi}} \right| d\boldsymbol{\xi}, \quad (101)
 \end{aligned}$$

where we have made the Taylor expansion $L_p(\zeta) - L_x(\zeta) = (\mathbf{p} - \mathbf{x}) \cdot \nabla_p L_p(\zeta) + \dots$ and have made the change of variables $(\omega, \zeta) \mapsto \boldsymbol{\xi} = 2\omega \nabla_p L_p(\zeta)/c$.

4.6. Diffraction tomography

In this case the data is the far-field pattern (34). Our inversion formula is (84), where $\tilde{s}_y = 1$ and there is no integration over t . The resulting formula is

$$I_{k_0}(\mathbf{p}) = \int e^{ik_0(\hat{\mathbf{z}}+\hat{\mathbf{y}}) \cdot \mathbf{p}} Q_{k_0}(\hat{\mathbf{z}}, \hat{\mathbf{y}}) F_\infty(\hat{\mathbf{y}}, \hat{\mathbf{z}}) d\hat{\mathbf{y}} d\hat{\mathbf{z}}, \quad (102)$$

where Q_{k_0} is the filter chosen according to [6],

$$Q_{k_0} = \frac{k_0^3}{(2\pi)^4} |\hat{\mathbf{y}} + \hat{\mathbf{z}}|, \quad (103)$$

which corrects for the Jacobian that is ultimately needed. Here the factor of k_0^3 corresponds to three-dimensional imaging.

The associated point-spread function is obtained from substituting (34) into (102),

$$\begin{aligned}
 I_{k_0}(\mathbf{p}) &= \int e^{ik_0(\hat{\mathbf{z}}+\hat{\mathbf{y}}) \cdot \mathbf{p}} Q_{k_0}(\hat{\mathbf{z}}, \hat{\mathbf{y}}) \int e^{-ik_0(\hat{\mathbf{z}}+\hat{\mathbf{y}}) \cdot \mathbf{x}} q(\mathbf{x}) d^3x d\hat{\mathbf{y}} d\hat{\mathbf{z}} \\
 &= \frac{k_0^3}{(2\pi)^4} \int e^{ik_0(\hat{\mathbf{z}}+\hat{\mathbf{y}}) \cdot (\mathbf{p}-\mathbf{x})} |\hat{\mathbf{z}} + \hat{\mathbf{y}}| d\hat{\mathbf{y}} d\hat{\mathbf{z}} q(\mathbf{x}) d^3x \\
 &= \int \chi_{2k}(\boldsymbol{\xi}) e^{i\boldsymbol{\xi} \cdot (\mathbf{p}-\mathbf{x})} d^3\xi q(\mathbf{x}) d^3x, \quad (104)
 \end{aligned}$$

where χ_{2k} denotes the function that is one inside the ball of radius $2k$ and zero outside and where we have used the Devaney identity [6]

$$\int \chi_{2k}(\boldsymbol{\xi}) e^{i\boldsymbol{\xi} \cdot \mathbf{r}} d^3\xi = \frac{k^3}{(2\pi)^4} \int_{S^2 \times S^2} e^{ik(\hat{\mathbf{y}}+\hat{\mathbf{z}}) \cdot \mathbf{r}} |\hat{\mathbf{y}} + \hat{\mathbf{z}}| d\hat{\mathbf{y}} d\hat{\mathbf{z}}. \quad (105)$$

The proof of this identity is outlined in the appendix. The two-dimensional version is [7]

$$\int \chi_{2k}(\boldsymbol{\xi}) e^{i\boldsymbol{\xi} \cdot \mathbf{r}} d^2\xi = \int_{S^1 \times S^1} e^{ik(\hat{\mathbf{y}}+\hat{\mathbf{z}}) \cdot \mathbf{r}} \left| \frac{\partial \boldsymbol{\xi}}{\partial(\hat{\mathbf{y}}, \hat{\mathbf{z}})} \right| d\hat{\mathbf{y}} d\hat{\mathbf{z}}, \quad (106)$$

where $\hat{\mathbf{y}} = (\cos \theta, \sin \theta)$, $\hat{\mathbf{z}} = (\cos \theta', \sin \theta')$ and

$$\left| \frac{\partial \boldsymbol{\xi}}{\partial(\hat{\mathbf{y}}, \hat{\mathbf{z}})} \right| = \sqrt{1 - (\hat{\mathbf{y}} \cdot \hat{\mathbf{z}})^2}. \quad (107)$$

4.7. Moving target tomography

Moving target tomography has been proposed in the paper [9], which models the signal using a simplified version of (21). For this simplified model, our imaging formula (70) reduces to the approach advocated in [9], namely matched-filter processing with a different filter for each location \boldsymbol{p} and for each possible velocity \boldsymbol{u} .

5. Conclusions and future work

We have developed a linearized imaging theory that combines the spatial, temporal and spectral aspects of scattered waves.

This imaging theory is based on the general (linearized) expression we derived for waves scattered from moving objects, which we model in terms of a distribution in phase space. The expression for the scattered waves is of the form of a Fourier integral operator; consequently, we form a phase-space image as a filtered adjoint of this operator.

The theory allows for activation of multiple transmitters at different times, but the theory is simpler when they are all activated so that the waves arrive at the target at roughly the same time.

The general theory in this paper reduces to familiar results in a variety of special cases. We leave for the future further analysis of the point-spread function. We also leave for the future the case in which the sensors are moving independently, and the problem of combining these ideas with tracking techniques.

Acknowledgments

This work was supported by the Office of Naval Research, by the Air Force Office of Scientific Research³ under agreement number FA9550-06-1-0017, by Rensselaer Polytechnic Institute, the Institute for Mathematics and its Applications, and by the National Research Council.

Appendix. The Devaney identity in \mathbb{R}^3

This proof of (105) follows [6]. First we note that for $\boldsymbol{r} \in \mathbb{R}^3$,

$$\begin{aligned} \int \frac{\chi_{2k}(\boldsymbol{\xi})}{|\boldsymbol{\xi}|} e^{i\boldsymbol{\xi} \cdot \boldsymbol{r}} d^3 \boldsymbol{\xi} &= \int_0^{2k} \int_{S^2} e^{i\boldsymbol{\xi} \cdot \boldsymbol{r}} d^2 \hat{\boldsymbol{\xi}} |\boldsymbol{\xi}| d|\boldsymbol{\xi}| \\ &= 4\pi \int_0^{2k} \frac{\sin |\boldsymbol{\xi}| r}{|\boldsymbol{\xi}| r} |\boldsymbol{\xi}| d|\boldsymbol{\xi}| \\ &= \frac{8\pi}{r^2} \frac{1 - \cos(2kr)}{2} = \frac{8\pi}{r^2} \sin^2 kr, \end{aligned} \quad (\text{A.1})$$

where we have written $r = |\boldsymbol{r}|$. Using Stone's formula [14]

$$\frac{\sin kr}{kr} = \frac{1}{4\pi} \int e^{ik\hat{\boldsymbol{y}} \cdot \boldsymbol{r}} d^2 \hat{\boldsymbol{y}}, \quad (\text{A.2})$$

we can write (A.1) as

$$\int \frac{\chi_{2k}(\boldsymbol{\xi})}{|\boldsymbol{\xi}|} e^{i\boldsymbol{\xi} \cdot \boldsymbol{r}} d^3 \boldsymbol{\xi} = \frac{k^2}{(2\pi)^2} \int e^{ik(\hat{\boldsymbol{y}} + \hat{\boldsymbol{z}}) \cdot \boldsymbol{r}} d^2 \hat{\boldsymbol{y}} d^2 \hat{\boldsymbol{z}}. \quad (\text{A.3})$$

³ Consequently, the US Government is authorized to reproduce and distribute reprints for Governmental purposes notwithstanding any copyright notation thereon. The views and conclusions contained herein are those of the authors and should not be interpreted as necessarily representing the official policies or endorsements, either expressed or implied, of the Air Force Research Laboratory or the US Government.

Next, we write

$$\begin{aligned} \int \chi_{2k}(\boldsymbol{\xi}) e^{i\boldsymbol{\xi} \cdot \mathbf{r}} d^3 \boldsymbol{\xi} &= \int \frac{\chi_{2k}(\boldsymbol{\xi})}{|\boldsymbol{\xi}|} e^{i\boldsymbol{\xi} \cdot \mathbf{r}} |\boldsymbol{\xi}| d^3 \boldsymbol{\xi} \\ &= \int e^{i\boldsymbol{\xi} \cdot \mathbf{r}} \left[\int e^{-i\boldsymbol{\xi} \cdot \mathbf{r}'} \left(\frac{k^2}{(2\pi)^4} \int e^{ik(\hat{\mathbf{y}} + \hat{\mathbf{e}}') \cdot \mathbf{r}'} d\hat{\mathbf{y}} d\hat{\mathbf{e}}' \right) \right] |\boldsymbol{\xi}| d^3 \boldsymbol{\xi} d\mathbf{r}'. \quad (\text{A.4}) \end{aligned}$$

Carrying out the \mathbf{r}' integration results in $\delta(\boldsymbol{\xi} - k(\hat{\mathbf{y}} + \hat{\mathbf{z}}))$; finally, carrying out the $\boldsymbol{\xi}$ integration results in (105).

References

- [1] Bleistein N, Cohen J K and Stockwell J W 2000 *The Mathematics of Multidimensional Seismic Inversion* (New York: Springer)
- [2] Borden B and Cheney M 2005 Synthetic-aperture imaging from high-Doppler-resolution measurements *Inverse Problems* **21** 1–11
- [3] Bradaric I, Capraro G T, Weiner D D and Wicks M C 2006 Multistatic radar systems signal processing *Proc. IEEE Radar Conf.*
- [4] Cooper J 1980 Scattering of electromagnetic fields by a moving boundary: the one-dimensional case *IEEE Antennas Propag.* **AP-28** 791–5
- [5] Cook C E and Bernfeld M 1967 *Radar Signals* (New York: Academic)
- [6] Devaney A J 1982 Inversion formula for inverse scattering within the Born approximation *Opt. Lett.* **7** 111–2
- [7] Devaney A J 1982 A filtered backpropagation algorithm for diffraction tomography *Ultrason. Imaging* **4** 336–50
- [8] Friedlander B and Porat B 1997 VSAR: a high resolution radar system for detection of moving targets *IEE Proc. Radar Sonar Navig.* **144** 205–18
- [9] Himed B, Bascom H, Clancy J and Wicks M C 2001 Tomography of moving targets (TMT) *Sensors, Systems, and Next-Generation Satellites V (Proc. SPIE vol 4540)* ed H Fujisada, J B Lurie and K Weber pp 608–19
- [10] Klemm R 2002 *Principles of Space-Time Adaptive Processing* (London: Institution of Electrical Engineers)
- [11] Levanon N 1988 *Radar Principles* (New York: Wiley)
- [12] Minardi M J, Gorham L A and Zelnio E G 2005 Ground moving target detection and tracking based on generalized SAR processing and change detection *Proc. SPIE* **5808** 156–65
- [13] Nolan C J and Cheney M 2002 Synthetic aperture inversion *Inverse Problems* **18** 221–36
- [14] Reed M and Simon B 1972 *Methods of Modern Mathematical Physics: I. Functional Analysis* (New York: Academic)
- [15] Soumekh M 1991 Bistatic synthetic aperture radar inversion with application in dynamic object imaging *IEEE Trans. Signal Process.* **39** 2044–55
- [16] Stuff M, Biancalana M, Arnold G and Garbarino J 2004 Imaging moving objects in 3D from single aperture synthetic aperture radar *Proc. IEEE Radar Conf.* pp 94–8
- [17] Swick D 1969 A review of wideband ambiguity functions *Naval Res. Lab. Rep.* **6994**
- [18] Tsao T, Slamani M, Varshney P, Weiner D, Schwarzlander H and Borek S 1997 Ambiguity function for a bistatic radar *IEEE Trans. Aerosp. Electron. Syst.* **33** 1041–51
- [19] Willis N J 1991 *Bistatic Radar* (Norwood, MA: Artech House)
- [20] Willis N J and Griffiths H D 2007 *Advances in Bistatic Radar* (Raleigh, NC: SciTech Publishing)
- [21] Willis N J 1990 Bistatic Radar *Radar Handbook* ed M Skolnik (New York: McGraw-Hill)
- [22] Woodward P M 1953 *Probability and Information Theory, with Applications to Radar* (New York: McGraw-Hill)
- [23] Yazici B, Cheney M and Yarman C E 2006 Synthetic-aperture inversion in the presence of noise and clutter *Inverse Problems* **22** 1705–29